Dynamics of photoexcited quasiparticles in heavy electron compounds

2006 J. Phys.: Condens. Matter 18 R281

(http://iopscience.iop.org/0953-8984/18/16/R01)

INSTITUTE OF PHYSICS PUBLISHING JOURNAL OF PHYSICS: CONDENSED MATTER

J. Phys.: Condens. Matter **18** (2006) R281–R314 doi:10.1088/0953-8984/18/16/R01

TOPICAL REVIEW

Dynamics of photoexcited quasiparticles in heavy electron compounds

Jure Demsar[1], John L Sarrao[2] and Antoinette J Taylor[2]

[1] Jozef Stefan Institute, Jamova 39, SI-1000, Ljubljana, Slovenia
[2] Los Alamos National Laboratory, Los Alamos, NM 87545, USA

E-mail: jure.demsar@ijs.si

Received 2 December 2005
Published 3 April 2006
Online at stacks.iop.org/JPhysCM/18/R281

Abstract

Femtosecond real-time spectroscopy is an emerging new tool for studying low energy electronic structure in correlated electron systems. Motivated by recent advances in understanding the nature of relaxation phenomena in various correlated electron systems (superconductors, density wave systems) the technique has been applied to heavy electron compounds in comparison with their non-magnetic counterparts. While the dynamics in their non-magnetic analogues are similar to the dynamics observed in noble metals (only weak temperature dependences are observed) and can be treated with a simple two-temperature model, the photoexcited carrier dynamics in heavy electron systems show dramatic changes as a function of temperature and excitation level. In particular, below some characteristic temperature the relaxation rate starts to decrease, dropping by more than two orders of magnitude upon cooling down to liquid He temperatures. This behaviour has been consistently observed in various heavy fermion metals as well as Kondo insulators, and is believed to be quite general. In order to account for the experimental observations, two theoretical models have been proposed. The first treats the heavy electron systems as simple metals with very flat electron dispersion near the Fermi level. An electron–phonon thermalization scenario can account for the observed slowing down of the relaxation provided that there exists a mechanism for suppression of electron–phonon scattering when both the initial and final electronic states lie in the region of flat dispersion. An alternative scenario argues that the relaxation dynamics in heavy electron systems are governed by the Rothwarf–Taylor bottleneck, where the dynamics are governed by the presence of a narrow gap in the density of states near the Fermi level. The so-called hybridization gap results from hybridization between localized moments and the conduction electron background. Remarkable agreement with the model suggests that carrier relaxation in a broad class of heavy electron systems (both metals and insulators) is governed by the presence of a (weakly temperature dependent) indirect hybridization gap.

Here we review the experimental results on a variety of heavy electron compounds, point out the common features as well as the peculiarities observed in some compounds, and compare the data with existing theoretical models.

(Some figures in this article are in colour only in the electronic version)

Contents

1. Introduction

Recent experiments have demonstrated that femtosecond time-resolved optical spectroscopy is a sensitive tool to probe the low energy electronic structure of strongly correlated electron systems, complementing conventional time-averaged frequency-domain methods. In these experiments, a femtosecond laser pulse excites a non-thermal electron distribution. These high energy electrons (holes) rapidly lose their energy via electron–electron (e–e) and electron–phonon (e–ph) scattering, reaching states near the chemical potential on the timescale of less than 100 femtoseconds (fs). This results in changes in the occupied density of states (DOS) in proximity to the Fermi energy (E_F), while further relaxation strongly depends on the peculiarities of the low energy electronic structure and the coupling strength between various degrees of freedom (electrons, lattice, spin...). By measuring photoinduced (PI) changes in optical properties as a function of temperature, excitation level, excitation frequency or applied external fields, it is possible to sensitively probe the nature of the electronic ground state. For example, measurements of the picosecond carrier relaxation dynamics of superconductors [1–3] and charge density wave compounds [4, 5] have shown that the presence of the gap in the density of states presents a relaxation bottleneck [2, 6], and that the magnitude of the gap can be extracted by analysing the temperature dependence of the photoexcited carrier density [1, 2]. Importantly, one of the main advantages of the real-time techniques is the ability to differentiate between various components based on their different timescales, different excitation intensity dependences or different probe matrix elements [7]. One such example is the observation of two distinct components in the response of cuprate superconductors,

implying the spatially inhomogeneous ground state [1, 7]. What is particularly important is that even though the probe photon energy in these experiments ranges from meV (the far-infrared spectral range) [8] up to several eV [9], the observed dynamics in these correlated electron systems are in many instances the same [3, 8], supporting the basic idea that regardless of the probe photon energy the states that are being probed lie in the vicinity of E_F.

Heavy fermion compounds present one of the challenging classes of materials in modern condensed matter physics, particularly due to their non-universal behaviour. A wide range of phenomena, such as unconventional superconductivity and non-Fermi liquid behaviour, have been reported. These various phenomena are believed to be a result of a competition between the single impurity physics (Kondo effect), correlations between local moments (lattice effects), band structure and crystal electric field effects [10]. Many heavy electron compounds are found to be well-described in terms of a single impurity model [10, 11], where their thermodynamics properties are governed by a single energy scale determined by a Kondo temperature T_K. In these systems, magnetic moments are localized at high temperatures and get screened by the conduction electrons when the temperature is lowered below T_K. However, intersite coupling between local moments can strongly affect the Kondo screening. The interplay between single impurity physics and lattice effects has presented itself as one of the long standing problems in condensed matter physics for decades, and an overall consensus is still lacking [10].

The main idea of studying the carrier relaxation dynamics in heavy electron systems using femtosecond time-resolved optical spectroscopy is to elucidate the effect of localized moments [10] on the quasiparticle relaxation dynamics, and obtain some complementary knowledge of the low energy electronic structure in these materials. To do this, we have performed systematic temperature and excitation intensity dependent studies on a variety of heavy fermion compounds $YbXCu_4$ (X = Ag, Cd, In), $CeCoIn_5$, $Yb_2Rh_3Ga_9$, and on the Kondo insulator SmB_6. A general feature in all studies is that the photoexcited carrier dynamics in heavy electron systems show dramatic changes as a function of temperature. In particular, below some temperature the relaxation rate starts to decrease, dropping in some cases by almost three orders of magnitude as the liquid He temperature is approached. Since this behaviour has been consistently observed in all the heavy electron systems studied thus far, it is believed to be quite general. In order to account for the experimental observations two theoretical models have been proposed. The first [12, 13] treats the heavy electron systems as simple metals with very flat electron dispersion near the Fermi level. This model shows that e–ph thermalization scenario can account for the observed slowing down of the relaxation provided that there is a mechanism of e–ph scattering suppression when both the initial and final electronic states lie within the energy range of flat dispersion [12, 13]. The alternative scenario [14] argues that the relaxation dynamics in heavy electron systems are governed by the presence of the hybridization gap (the hybridization between localized moment and conduction electrons leads to opening of the hybridization gap), where the low temperature slowing down of relaxation is due to the Rothwarf–Taylor phonon bottleneck mechanism [15, 16].

In this paper, we first review the experimental results on the temperature dependence of the photoexcited carrier relaxation dynamics obtained on a variety of heavy electron compounds in the low excitation density limit. This is followed by experimental data on the excitation intensity dependence of the relaxation dynamics taken at low temperatures. Utilizing a low repetition rate amplified laser system, the excitation intensity was varied over more than three orders of magnitude, revealing strong dependence of the relaxation processes on the perturbation level. In the next section the experimental data are compared with the two theoretical models developed to explain the dynamics of photoexcited carriers in these compounds [12, 14]. This is followed by a summary and discussion of future perspectives.

2. Experimental details

2.1. Experimental configuration

For the low excitation intensity experiments we used a standard pump–probe set-up with a mode-locked Ti:sapphire laser producing 20 fs pulses centred at 800 nm (photon energy $\hbar\omega_{\rm ph} \simeq 1.55$ eV) with an 80 MHz repetition rate. The probe photon energy was varied between 1.5 and 1.62 eV with no detectable variation in the photoinduced change. The PI changes in reflectivity $\Delta R/R$ were measured using a photodiode and lock-in detection. The pump fluence was kept below 1 μJ cm^{-2} and the pump/probe intensity ratio was $\sim$30. The base temperature was varied between 4 and 350 K by utilizing a continuous flow optical cryostat. The pump fluence was kept below 1 μJ cm^{-2} for two reasons: (a) to keep the system as close to equilibrium as possible and (b) to minimize the overall heating of the illuminated spot [17]. Steady-state heating effects were accounted for as described in section 2.2, yielding an uncertainty in temperature of less than 3 K (in all of the data the temperature increase of the illuminated spot has been accounted for).

When performing studies of the excitation fluence (F) dependence of the dynamics at low temperatures, while minimizing the continuous heating of the probed spot due to laser excitation, we used a commercial regeneratively amplified Ti:sapphire laser system (diode pumped RegA 9050 from Coherent Inc.) and an optical parametric amplifier (OPA 9450 from Coherent Inc.) operating at 250 kHz producing sub-100 fs pulses. The samples were excited at 3.0 eV with F ranging from 0.5 to 600 μJ cm^{-2}, while the photoinduced changes in reflectivity were measured at the photon energy of 1.67 eV. The choice of 3 and 1.67 eV photon energies for pump and probe, respectively, was mandated by the requirement for a wide range of excitation intensities and a good signal-to-noise ratio over the entire F-range. Therefore, the experiment was performed in a two color pump–probe configuration. The residual pump second harmonic output from the OPA at 3 eV enabled the widest range of excitation intensities, while the 1.67 eV signal beam from the OPA was the closest we could get to the 1.55 eV used in the high repetition rate system. Importantly, the lowest F used in this study was only about a factor of 5 higher than the fluences used in the low excitation density study, while the maximum F is more than 1000 times higher. We should note that, since the repetition rate of the amplified system is three orders of magnitude lower then in the high repetition rate system [12], the effect of continuous heating is minimized.

The samples studied in this research were high purity single crystals grown by the flux method [18]. Experiments were performed on either as grown or freshly polished single crystals, the results being independent of the preparation.

2.2. Steady-state heating effects

Continuous heating of the illuminated laser spot in the experiments with high repetition laser systems can be substantial, particularly at low temperatures when thermal conductivity is low. Since the dynamics in these compounds are strongly temperature dependent, the effect of continuous heating has to be accounted for before analysing the temperature dependences of various parameters extracted from fits and data analysis in terms of various theoretical models.

One can estimate the steady-state heating of the illuminated spot by considering the temperature increase ΔT induced by illumination with a continuous laser of the same average power density. Since sample thicknesses ($\sim$0.3–1 mm) are typically much larger than the optical absorption length ($\sim$10–40 nm) the temperature rise can be calculated using a simple steady-state heat diffusion model for a semi-infinite solid [19], where the Gaussian laser beam with the average laser power P is focused onto a spot with diameter d (the Gaussian

beam waist) on the semi-infinite solid with reflectivity R, absorption coefficient α, and thermal conductivity κ (here we consider cubic symmetry). With $z = 0$ on the surface, and the centre of the Gaussian beam being chosen as the origin of the coordinate system, the boundary condition is that the temperature at $z = \infty$ is equal to the temperature of the cold finger. Since we are dealing with temperature rises of the order of 5–10 K we can neglect the energy loss due to thermal radiation. Using this model one obtains the expression for the temperature rise [20]

$$\Delta T\,(x, y, z) = \frac{\alpha\,(1-R)}{2\pi^2 d^2 k^3} \int_0^{2\pi} \mathrm{d}\phi \int_0^{\infty} \rho\,\mathrm{d}\rho\,\mathrm{e}^{-\left(\frac{\sqrt{2}x}{d}-\frac{\sqrt{2}\rho\cos\phi}{kd}\right)^2-\left(\frac{\sqrt{2}y}{d}-\frac{\sqrt{2}\rho\sin\phi}{kd}\right)^2} \times \left[\mathrm{e}^{\alpha z}\int_{kz}^{\infty}\frac{\mathrm{e}^{-\frac{\alpha\tilde{z}}{k}}}{\sqrt{\rho^2+\tilde{z}^2}}\,\mathrm{d}\tilde{z} + \mathrm{e}^{-\alpha z}\int_{-\infty}^{kz}\frac{\mathrm{e}^{\frac{\alpha\tilde{z}}{k}}}{\sqrt{\rho^2+\tilde{z}^2}}\,\mathrm{d}\tilde{z}\right], \tag{1}$$

where $k = \kappa/P$. In $YbAgCu_4$ at 1.5 eV $R \approx 0.7$, while the real and imaginary optical conductivities are $\sigma_1 \approx 2400\ \Omega^{-1}\ \mathrm{cm}^{-1}$ and $\sigma_2 \approx 4100\ \Omega^{-1}\ \mathrm{cm}^{-1}$ [21], giving the absorption coefficient[3] $\alpha \approx 7 \times 10^7\ \mathrm{m}^{-1}$ (the same absorption coefficient is also obtained at 3 eV). At 5 K the thermal conductivity is $\kappa \approx 3\ \mathrm{W\,mK}^{-1}$ [22]. With $d = 50\ \mu\mathrm{m}$ and $P = 10$ mW (corresponding to $F = 6\ \mu\mathrm{J\,cm}^{-2}$) the temperature increase $\Delta T(0, 0, 0) \sim 8$ K is obtained. This number should be taken as a rough estimate of heating, since apart from some uncertainty in the values of κ, α and R, a small error in determining the laser beam parameter (d) can also change ΔT. Moreover, the calculation assumes the thermal conductivity to be temperature independent over the temperature range between the cold finger temperature T_0 and $T_0 + \Delta T$, which is generally not the case. Therefore this calculation should be performed iteratively. In the case when κ increases with temperature (as is the case in $YbAgCu_4$ over the entire temperature range of studies), ΔT estimated from equation (1) presents an upper limit for the temperature increase. What follows from this estimate is that if the fluence is kept under $1\ \mu\mathrm{J\,cm}^{-2}$ the temperature increase in the illuminated spot is under 2 K.

2.3. Data analysis

A typical time-resolved photoinduced reflectivity signal measured in these experiments is shown in figure 1.

Here zero on the horizontal axis represents the time when the photoexcitation pulse excites the sample. Therefore at negative time delays (before photoexcitation), the photoinduced signal is zero. After (and during) photoexcitation the reflectivity starts to change and in a characteristic time τ_r the photoinduced change is maximized. This is followed by the decay of the photoinduced reflectivity on the picosecond timescale.

In addition to the picosecond dynamics, a component decaying on a much longer timescale ($\gg$ns) is often observed, manifested as a plateau (offset) at long time delays. This slowly decaying component is commonly attributed to the simple bolometric response, where the reflectivity change ($\Delta R = \frac{\partial R}{\partial T}\Delta T$) reflects the change in the sample temperature, ΔT, following photoexcitation and thermalization of all the subsystems. Decay, governed by the heat diffusion out of the excited volume, proceeds on the nanosecond timescale. When the reflectivity does not have a very pronounced temperature dependence, i.e. when $\frac{\partial R}{\partial T}$ is approximately constant, the amplitude of this offset is the highest at low temperatures, when the specific heat is the lowest. This kind of temperature dependence is commonly observed in metals.

Quite generally, the purpose of these kinds of measurement in various strongly correlated electron systems is to determine the microscopic mechanism of carrier relaxation processes. This is achieved by systematic studies of the dynamics as a function of temperature, excitation

[3] From optical reflectivity data on $YbAgCu_4$ [21] it follows that at 1.5 eV $\varepsilon_1 \approx -20$, $\varepsilon_2 \approx 12$ which gives the optical penetration depth of ≈15 nm.

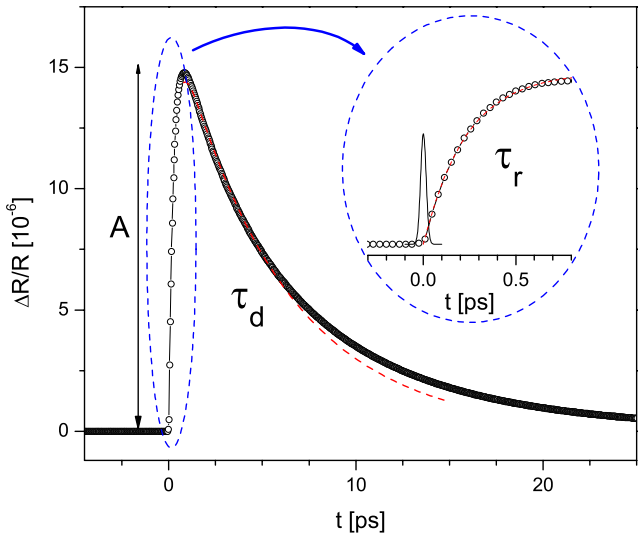

Figure 1. Typical shape of the time-resolved photoinduced reflectivity signal obtained by femtosecond optical techniques. The observables that are being discussed and further analysed are the amplitude of the transient A, the decay (or relaxation) time τ_d, and the rise-time τ_r (if it is not resolution limited, i.e. if it is much longer that the duration of optical pulse as in the above case). The dashed line in the inset presents the fit of the rising edge with $A(1 - \exp(-t/\tau_r))$. To fit the decay dynamics an exponential decay function is usually used (dashed line). However, quite often the decay is non-exponential (as in this illustration), and in this case other (model dependent) decay fit functions are used.

level and applied external fields, and by analysing the effect of varying various parameters on the photoinduced transient. The simplest fitting function that can be used to analyse the data is

$$\Delta R(t)/R = H(t)[Ae^{-t/\tau_d} + C]. \tag{2}$$

Here $H(t)$ is a function that describes the finite rise-time (τ_r), C is the long-lived bolometric signal which is considered to be constant on the 100 ps timescale, while A and τ_d are the amplitude and the decay time of the electronic response. The rise-time is often limited by the duration of the optical excitation pulse. In this case $H(t)$ is the Heaviside function convoluted with the Gaussian $\exp(2t^2/\tau_p^2)$, where τ_p is the optical pulsewidth. In case the rise-time of the photoinduced reflectivity signal is substantially longer then τ_p, $H(t)$ is given by the Heaviside function multiplied by a $1 - \exp(-t/\tau_r)$ term, which describes the rising edge of the photoinduced transient. In the following, we will focus on the picosecond and sub-picosecond electronic response, where the observables that are being measured as a function of temperature, excitation level, or applied external field are the amplitude of the transient (denoted by A in figure 1), the rise-time τ_r (if longer than experimental resolution determined by the length of the optical pump and probe pulses), and the decay time τ_d.

While the decay dynamics can often be well approximated by a single exponential decay (as in the case demonstrated in figure 1), the departure from e^{-t/τ_d} behaviour is often quite pronounced. It can be attributed either to the underlying microscopic mechanism, as is the case for the photoinduced carrier relaxation dynamics in narrow gap systems [14, 16], or to extrinsic effects, like disorder or structural inhomogeneity. Moreover, the departure from exponential decay dynamics is quite generally expected at low temperatures, since at low enough temperatures a crossover from the weak to the strong perturbation limit is expected (e.g. at low enough temperatures the density of photogenerated electron–hole pairs becomes

higher than the density of thermally excited electron–hole pairs). In this case the exponential decay fit may still represent the (qualitative) first approximation. In some cases, however, the relaxation dynamics are found to be strongly non-exponential over the entire temperature and/or excitation intensity range. In the case when normalizing the data to the value of the photoinduced reflectivity maximum and scaling the time axis to some effective decay time shows that the functional form of relaxation does not vary with temperature and/or excitation level, one can argue that the non-exponential relaxation occurs due to some underlying microscopic mechanism [5]. Since the microscopic mechanism is to be determined based on the dependence of typical timescales on temperature, excitation level, and external field, the initial goal is to describe the dynamics with a *minimal* set of parameters. A stretched exponential functional form, $\mathsf{A}\exp[-(t/\tau_{\mathrm{d}}^{\mathrm{eff}})^{p}]$, can often be used to describe the decay dynamics. This functional form is commonly used to describe the relaxation process, where relaxation is governed by some distribution of relaxation rates which may result due to sample inhomogeneity or crystal anisotropy[4] for example. Here $\tau_{\mathrm{d}}^{\mathrm{eff}}$ is some effective decay time, while p is the stretching parameter, which can take values $0 < p < 1$ [24]. It should be noted that smaller values of p correspond to a broader distribution of relaxation rates. For example $p \approx 0.9$ corresponds to a nearly exponential relaxation with the decay time $\approx\tau_{\mathrm{d}}^{\mathrm{eff}}$, while in the case of $p \approx 0.5$ the decay times span approximately one order of magnitude with the most probable decay time (peak in the distribution function of decay rates) $\approx 2\tau_{\mathrm{d}}^{\mathrm{eff}}$; see [24] for further details.

In the following sections, we present the systematic studies of the photoinduced reflectivity transients in various heavy electron compounds as a function of temperature (section 2.4) and excitation level (section 2.5), in order to determine the general trends in the behaviour of photoinduced carrier density and (effective) decay rate. When applicable, a single exponential decay function (equation (2)) is used to fit the data. In case the departure from the single exponential decay function is pronounced, a stretched exponential decay function is used to analyse the data and to extract the effective relaxation rate.

2.4. Experimental results obtained in the low excitation density regime

In this section we summarize the main experimental observations. First we compare the temperature dependences of the relaxation dynamics taken in the low excitation limit on a heavy fermion $YbAgCu_4$ compared to the non-magnetic $LuAgCu_4$ to emphasize the difference in their responses. Second, we summarize the results on several heavy fermion metals together with the Kondo insulator SmB_6, pointing out the common features and some differences.

2.4.1. The T-dependence of relaxation dynamics on heavy fermion $YbAgCu_4$ compared to the non-magnetic $LuAgCu_4$. In order to study the carrier relaxation dynamics in heavy electron compounds we have performed measurements of the temperature dependence of the photoinduced reflectivity on $YbAgCu_4$. $YbAgCu_4$ is cubic, and it is a prototypical heavy fermion (HF) system characterized by a Kondo temperature $T_{\mathrm{K}} \sim 100$ K [25]. Its thermodynamic properties are well described within the single-impurity limit [10, 11]. $YbAgCu_4$ possesses a low temperature Sommerfeld coefficient γ, defined as the heat capacity C divided by the temperature T in the low temperature limit, of $\sim$200 mJ mol^{-1} K^{-2}. We contrast the photoinduced behaviour of $YbAgCu_4$ with that of $LuAgCu_4$, its non-magnetic analogue (with $\gamma \sim 10$ mJ mol^{-1} K^{-2}). The experiments were performed on freshly polished flux-grown single crystals [25] in the low excitation density limit.

[4] Recent analysis of the optical conductivity data on various heavy electron compounds [23] points to strong anisotropy of the low energy electronic structure in these compounds.

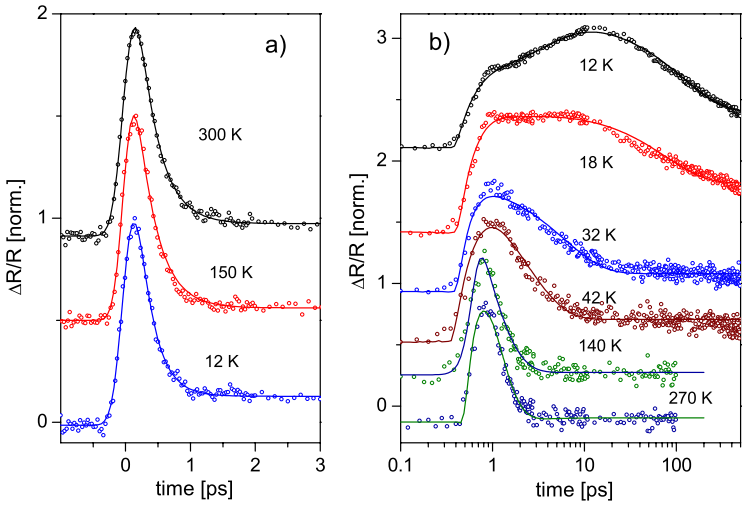

Figure 2. Normalized photoinduced reflectivity data on (a) $LuAgCu_4$ and (b) $YbAgCu_4$ at various temperatures. The experimental data are presented by open circles, while theoretical fits are shown as solid lines. The data have been vertically shifted for clarity. Note that the data on $YbAgCu_4$ are plotted on the semi-logarithmic plot due to the more than two orders of magnitude change in relaxation rate between 10 and 300 K.

Figure 2 presents the photoinduced reflectivity data for $LuAgCu_4$ and for the heavy fermion $YbAgCu_4$ at several temperatures between ≈10 and 300 K. The relaxation dynamics of the non-HF compound $LuAgCu_4$ display a very weak temperature dependence, with $\Delta R/R$ recovering on a sub-picosecond timescale at all temperatures[5]. The recovery dynamics are well described by a single exponential decay (solid lines are fits to the data) similar to regular metals such as Au and Ag [26], where the recovery is predominantly due to e–ph thermalization. In contrast, figure 2(b) shows that in $YbAgCu_4$ the quasiparticle dynamics are strongly temperature dependent. Specifically, above ∼140 K, the decay is virtually temperature independent but increases by more than two orders of magnitude as $T \rightarrow 0$ K. The decay dynamics are in both cases well approximated by a single exponential decay function $\mathrm{A}\exp(-t/\tau_\mathrm{d})$; the solid lines in figure 2 represent fits to the data by a single exponential decay. The temperature dependence of the decay time τ_d extracted by an exponential decay fit is plotted in figure 3. As shown in subsections 2.4.2–2.4.5, similar behaviour has been observed in $YbCdCu_4$, $CeCoIn_5$, $Yb_2Rh_3Ga_9$, as well as in the Kondo insulator SmB_6, implying that the slowing down of the relaxation at low temperatures first observed in $YbAgCu_4$ is apparently a generic feature of the heavy electron systems and derives from their low energy electronic structure.

Apart from the dramatic decrease in the relaxation rate in $YbAgCu_4$, we should also mention the pronounced temperature dependence of the amplitude of the transient, and, in particular, the peculiar rise-time dynamics observed in $YbAgCu_4$. For $LuAgCu_4$, the rise-time is ∼100 fs at all temperatures. This is again similar to what has been observed in conventional metals [26, 27] and reflects the time it takes for the initially created high energy quasiparticles to thermalize towards E_F. Above ∼25 K, $YbAgCu_4$ displays a similar (fast) rise-time. Below 25 K the rise-time increases and, as the semi-log plot in figure 2(b) reveals, reflects a two-step

[5] The picosecond recovery dynamics are followed by slow relaxation on the nanosecond timescale, attributed to a simple bolometric response (see section 2.3).

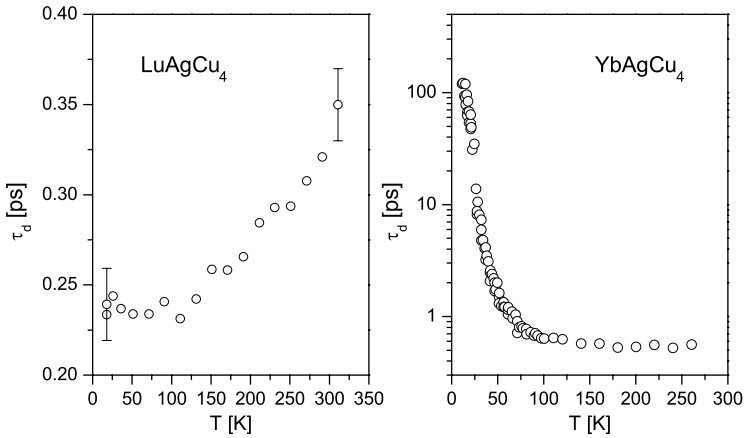

Figure 3. The temperature dependence of the decay time τ_d for the heavy fermion metal $YbAgCu_4$ and its non-magnetic counterpart $LuAgCu_4$. Note the semi-logarithmic scale in the case of $YbAgCu_4$.

process at the lowest temperatures. Similar behaviour is also observed in $CeCoIn_5$, while in $YbCdCu_4$ and $Yb_2Rh_3Ga_9$ no anomalous rise-time dynamics are observed down to the lowest temperatures. As will be shown later, these peculiar rise-time dynamics can be accounted for within the phonon-bottleneck scenario, discussed in section 3.2.

2.4.2. Photoexcited carrier dynamics in $YbCdCu_4$. $YbCdCu_4$ is an isostructural heavy fermion compound in the $YbXCu_4$ series [25]. It is characterized by a similar Kondo energy scale ($T_K \sim$ 100–200 K [25]) and low temperature Sommerfeld coefficient ($\gamma \sim$ 175 mJ mol^{-1} K^{-2}) similar to $YbAgCu_4$. On the other hand, the residual resistivity in $YbCdCu_4$ is almost an order of magnitude higher than in $YbAgCu_4$, which implies that $YbCdCu_4$ is a rather bad metal compared to $YbAgCu_4$. In fact, it follows from the analysis of the transport data [25] that the conduction electron bandwidth is about five times smaller in $YbCdCu_4$ than in $YbAgCu_4$. Thus, comparing the photoinduced response in $YbAgCu_4$ and $YbCdCu_4$ allows us to examine the role of the conduction electron density of states on the relaxation phenomena.

Figure 4 presents the temperature dependence of the photoinduced reflectivity dynamics in $YbCdCu_4$ measured in the low excitation density regime. Similar to $YbAgCu_4$, the relaxation dynamics show a dramatic slowing down upon cooling. Unlike in $YbAgCu_4$ the decay dynamics are strongly non-exponential, which can be seen directly from the raw data. In fact the dynamics can be well accounted for by a stretched exponential decay $\mathsf{A}\exp[-(t/\tau_d^{\mathrm{eff}})^p]$ with stretching power $p \approx 1/3$ over the entire temperature range. Moreover, no picosecond rise-time dynamics are observed down to the lowest temperatures and excitation intensities. The most probable reason for the absence of the peculiar rise-time dynamics as observed in $YbAgCu_4$ is the fact that the span of the decay timescales is very large ($p = 1/3$ corresponds to a broad distribution of decay times over two orders of magnitude with the most probable decay time of $\approx$10–20τ_d^{eff} [24]). Therefore, even though the overall recovery proceeds on the 100 ps timescale the fastest processes can cut off the rise-time dynamics.

It is noteworthy that even though the absolute values of the most probable decay time in $YbCdCu_4$ (which is $\approx$10–20τ_d^{eff}) and τ_d in $YbAgCu_4$ are not the same, the temperature dependences of the two are quite similar; see figure 5.

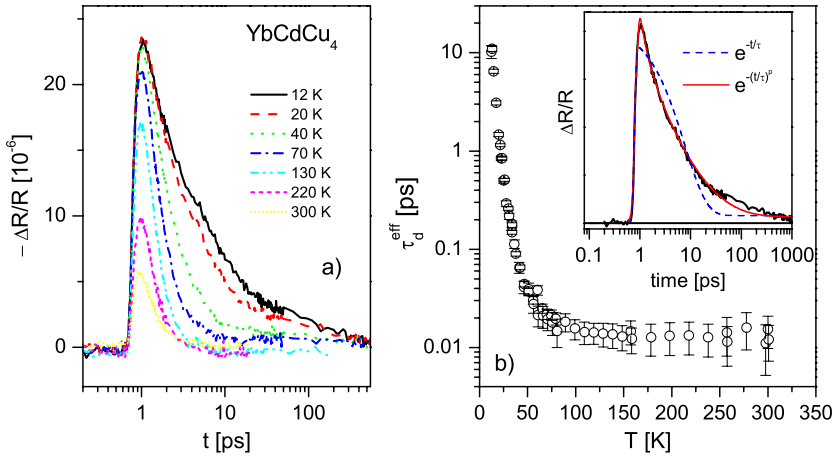

Figure 4. (a) The temperature dependence of the photoinduced reflectivity dynamics in $YbCdCu_4$ taken in the low excitation density experimental configuration. From the low temperature trace it is clear that the relaxation dynamics are strongly non-exponential. (b) The temperature dependence of the effective decay time $\tau_d^{\rm eff}$ extracted by fitting the recovery dynamics with a stretch exponential with $p = 1/3$ over the entire temperature range. The inset to panel (b) shows the comparison of the fit of the low temperature data with both single exponential and the stretch exponential decay.

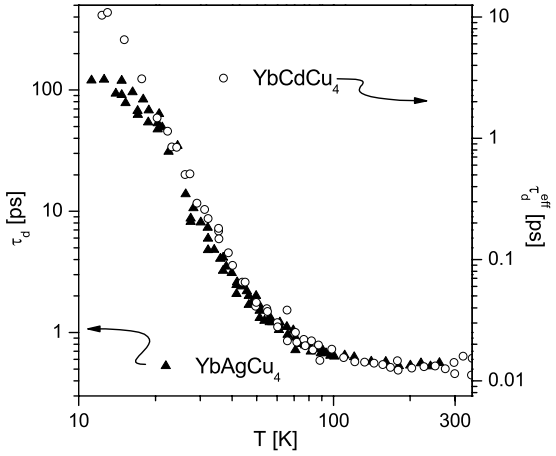

Figure 5. Comparison of the temperature dependence of the decay times in $YbAgCu_4$ and $YbCdCu_4$. Even though the absolute values of the two timescales differ (note that $\tau_d^{\rm eff}$ is an effective time), the temperature dependences of the two exhibit a remarkable similarity.

2.4.3. Photoexcited carrier dynamics in $Yb_2Rh_3Ga_9$. Spectroscopic data on $YbXCu_4$ (X = Au, Ag, Cd, ...) imply that there is a common underlying electronic structure in these compounds, which is relatively independent of X [25]. Their electronic structure is characterized by a pseudogap in the density of states; by varying X only the position of the Fermi level is changed. $Yb_2Rh_3Ga_9$ is a somewhat different ytterbium-based heavy fermion system [28]. $Yb_2Rh_3Ga_9$ crystallizes in a hexagonal structure, and modest magnetic anisotropy is observed. Importantly, the crystal electric field splitting is of the order of the Kondo temperature, leading to a non-trivial temperature dependence of magnetic susceptibility [28].

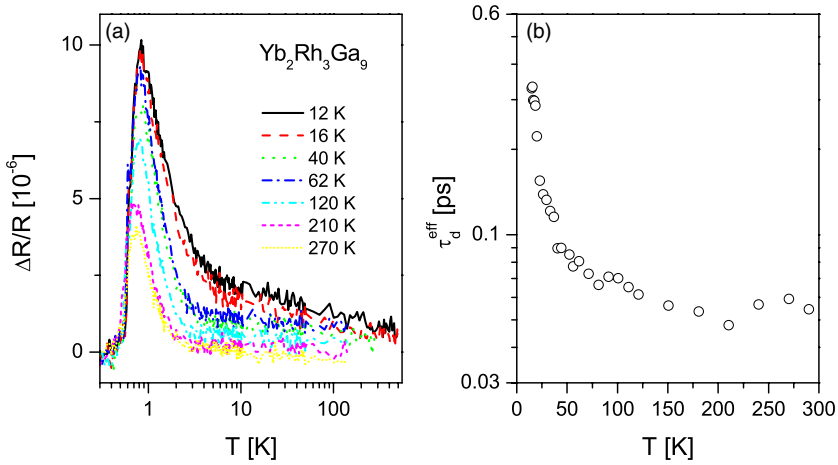

Figure 6. (a) The temperature dependence of the photoinduced reflectivity dynamics on $Yb_2Rh_3Ga_9$ taken in the low excitation density experimental configuration. It is clear that also in $Yb_2Rh_3Ga_9$ the decay dynamics are strongly non-exponential. (b) The temperature dependence of the effective decay time τ_d^{eff} extracted by fitting the recovery dynamics with a stretched exponential with $p = 0.4$ over the entire temperature range.

Usually, in cases when crystal field splitting is present, the hybridization between conduction electrons and any of the magnetic configurations $|m\rangle$ of the local moment is taken to be independent of $|m\rangle$. This approximation is successfully applied even though different orientations of orbitals with respect to the nearest neighbour atoms should give rise to differences in hybridization, affecting the magnetic and transport properties. In $Yb_2Rh_3Ga_9$, however, this procedure failed when describing the magnetic susceptibility data [28, 29], and the crystal electric field effects had to be taken into account. By measuring the photoexcited carrier relaxation dynamics in $Yb_2Rh_3Ga_9$ one can study the effect of crystal field splitting on the relaxation dynamics.

Figure 6 presents the temperature dependence of the photoinduced reflectivity dynamics in $Yb_2Rh_3Ga_9$ measured in the low excitation density regime. While the slowing down of the relaxation upon cooling is not as pronounced as in $YbAgCu_4$ or $YbCdCu_4$, the effect is still clearly observed. Furthermore, the decay dynamics are again strongly non-exponential and can be well accounted for by the stretch exponential decay $\mathrm{A}\exp[-(t/\tau_d^{\text{eff}})^p]$ with stretching power $p \approx 0.4$ over the entire temperature range. As in $YbCdCu_4$, no picosecond rise-time dynamics are observed all the way to the lowest temperatures and excitation intensities, and similar reasoning can be used to account for the absence of the peculiar rise-time dynamics as observed in $YbAgCu_4$.

2.4.4. Photoexcited carrier dynamics in $CeCoIn_5$. $CeCoIn_5$ is a tetragonal heavy fermion compound that happens to have the highest critical temperature of heavy fermion superconductors [30]. It is a very good metal with residual resistivity less than 1 $\mu\Omega$ cm and Sommerfeld coefficient $\gamma \approx 1000$ mJ mol^{-1} K^{-2} [31]. Important to our studies, $CeCoIn_5$ appears to display strong intersite coupling between the screened local moments at low temperatures [32] that gives rise to a form of two-fluid behaviour [33]. The characteristic energy scale of intersite coupling of $T^* \approx 50$ K was found to be substantially lower than the crystal level splitting $\Delta \approx 120$ K [32].

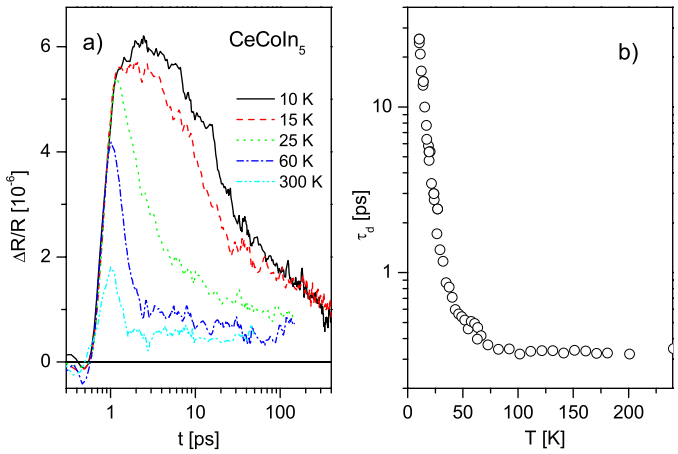

Figure 7. (a) The temperature dependence of the photoinduced reflectivity dynamics of the heavy fermion $CeCoIn_5$ measured in the low excitation density regime. (b) The temperature dependence of the decay time τ_d extracted by fitting the recovery dynamics with an exponential decay function.

The results of our ultrafast photoinduced carrier dynamics studies of $CeCoIn_5$ are plotted in figure 7. The relaxation dynamics can over most of the temperature range be well fitted by the single exponential decay. Only at temperatures below ≈20 K, is the best fit achieved with a stretched exponential with $p \approx 0.7$. For simplicity, the decay time obtained with a single exponential decay fit is plotted in panel (b). Similar to all compounds studied, the (initial) decay time dramatically increases (by two orders of magnitude) upon cooling. The amplitude of the transient also shows a pronounced temperature dependence, decreasing upon increasing the temperature. Moreover, comparing the temperature dependence of the decay time with $Yb(Ag, Cd)Cu_4$ or $Yb_2Rh_3Ga_9$, one can see that the crossover temperature where the decay time starts to show a pronounced temperature dependence is considerably lower in $CeCoIn_5$. We should emphasize one of the aspects of the data in comparison with other heavy electron compounds. Namely, at low enough temperatures two-stage rise-time dynamics are consistently observed, similar to $YbAgCu_4$.

2.4.5. Photoexcited carrier dynamics in Kondo insulator SmB_6. SmB_6 is cubic and displays quasi-insulating behaviour at low temperatures. It is widely accepted that this semiconducting behaviour arises from correlation effects, and SmB_6 is considered a prototypical Kondo insulator compound [34, 35]. As such, it is an important benchmark compound for our photoexcited carrier relaxation studies.

Figure 8 shows the temperature dependence of the photoinduced reflectivity change in SmB_6 taken in the low excitation density regime. The trend in relaxation dynamics is the same as that observed in heavy fermion metals, showing that the observed phenomenon is a general phenomenon in heavy electron systems. The relaxation is, like in many of the studied heavy fermion compounds, found to be non-exponential, with the decay dynamics well described by a stretched exponential decay function $\mathrm{A}\exp[-(t/\tau_d^{\mathrm{eff}})^p]$, with stretching power $p = 0.58$. The effective decay time τ_d^{eff} increases by nearly two orders of magnitude upon cooling and is similar to the decay time in heavy fermion metals in which the relaxation was found to be a stretched exponential. No two-step rise-time is observed down to the lowest temperatures measured.

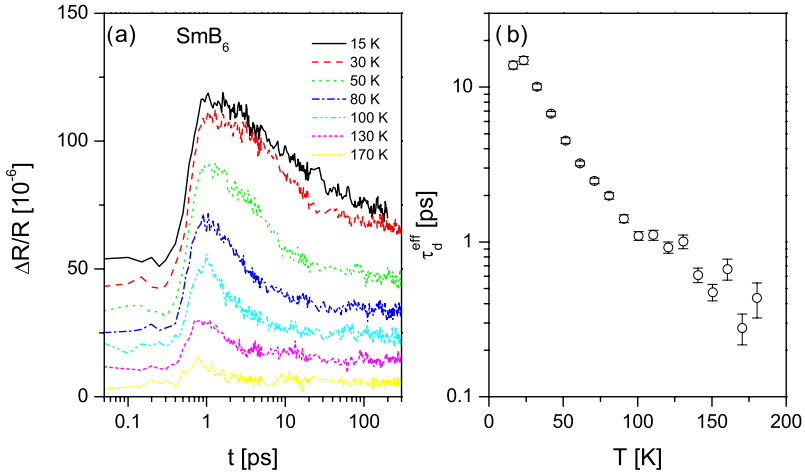

Figure 8. (a) The temperature dependence of the photoinduced reflectivity dynamics in the Kondo insulator SmB_6 in the low excitation density regime. The data are vertically shifted for clarity. (b) The temperature dependence of the effective decay time τ_d^{eff} extracted by fitting the recovery dynamics with a stretch exponential decay function (stretching power of 0.58 was used).

2.5. Low temperature excitation intensity dependence studies

In ultrafast real-time spectroscopies, often called pump–probe techniques, one characteristic of the approach is that the system investigated is no longer in thermodynamic equilibrium (even though this deviation might be marginal in some cases, for example at extremely low excitation densities). Therefore, the variation of the excitation level presents an additional experimental parameter, and the dependence of the relaxation phenomena on the excitation intensity can present an additional constraint for the theoretical description of the relaxation processes.

When performing excitation intensity dependent studies of the relaxation dynamics one needs to be aware of possible artefacts. For example, the excitation of the sample with laser pulses gives rise to a steady-state temperature increase. Steady-state heating is particularly pronounced at low temperatures, when thermal conductivity is low. Therefore, in cases where the decay dynamics at low temperatures are strongly temperature dependent (as is the case in heavy electron systems [12, 13] or superconductors [16]), the measured excitation intensity dependence can be entirely due to the fact that the steady-state temperature of the illuminated spot varies as a function of the excitation level.

By carefully performing temperature dependence studies at different excitation levels, the steady-state heating effect can be accounted for [17]. Since there is a simple connection between the temperature increase, ΔT, thermal conductivity κ and excitation power P (i.e. $\Delta T \propto P/\kappa$), one can easily test whether the photoexcitation intensity dependence of the relaxation dynamics is intrinsic or is merely due to the heating of the probed spot. Indeed, in case of experiments performed in the low excitation density regime with a high repetition rate laser system, continuous heating was found to dominate the excitation intensity dependence. To put this in numbers, in $YbAgCu_4$ where at $\approx$10 K the thermal conductivity is $\approx$5 W mK^{-1} [22], an excitation with 3 mW of average power, focused to a $\approx$70 μm diameter spot (which corresponds to an excitation fluence (F) of $F \approx 0.1$ μJ cm^{-2}) gives rise to a temperature increase of $\approx$5 K.

In order to study the excitation intensity dependence of the dynamics at low temperatures, while minimizing the continuous heating of the probed spot due to laser excitation, we used a

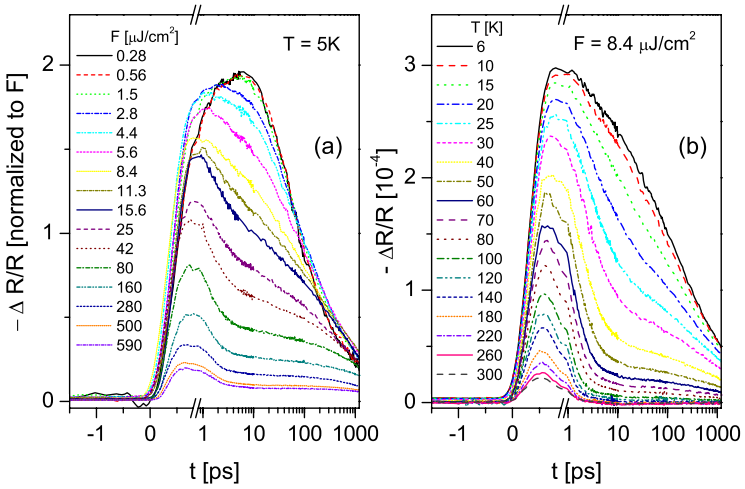

Figure 9. (a) Photoexcitation fluence (F) dependence of the photoinduced reflectivity transient in $YbAgCu_4$ at 5 K. The data have been normalized to F to emphasize the sub-linear F-dependence of the amplitude. (b) The T-dependence of the PI reflectivity measured at $F = 8.4\ \mu J\ cm^{-2}$.

commercial regeneratively amplified Ti:Al_2O_3 laser system and an optical parametric amplifier operating at 250 kHz and producing sub-50 fs pulses. The experiments were performed using a standard pump–probe set-up. The samples were excited at 3.0 eV with an excitation fluence ranging from 0.5 to 600 $\mu J\ cm^{-2}$, while the photoinduced changes in reflectivity were measured at the photon energy of 1.67 eV. Importantly, the lowest fluences used in this study were only about a factor of five higher then the fluences used in the earlier study [12], while the maximum fluence was more than three orders of magnitude higher. On the other hand, since the repetition rate of the amplified system is almost three orders of magnitude lower than in the high repetition rate system, the effect of continuous heating is minimized, i.e. the temperature rise of the illuminated spot at the fluence of 160 $\mu J\ cm^{-2}$ is only about 5 K, comparable to the continuous temperature rise in the experimental configuration with the high repetition laser system using $F \approx 0.1\ \mu J\ cm^{-2}$.

Figure 9(a) presents the photoinduced reflectivity in $YbAgCu_4$ measured at 5 K while F is varied from 0.28 to 580 $\mu J\ cm^{-2}$. All of the reflectivity transients are normalized to F. At the lowest F, the data are consistent with the low-T data obtained in the low excitation density configuration [12]. The initial (resolution limited) rise-time is followed by a further rise of the signal on a picosecond timescale. The recovery dynamics proceed on a 100 ps timescale. The decay dynamics are only weakly F-dependent up to $\approx 4\ \mu J\ cm^{-2}$. This is consistent with the excitation intensity dependence measurements in the low excitation density/high repetition rate configuration, where the dynamics were found to be independent of the excitation density.

As the fluence F is further increased, the photoinduced transient is dramatically changed. The second-step picosecond rise-time dynamics become faster, and above $F \approx 4\ \mu J\ cm^{-2}$, the overall rise-time is resolution limited. The decay time also rapidly increases above $F \approx 4\ \mu J\ cm^{-2}$, by almost two orders of magnitude. Moreover, the amplitude of the transient A exhibits linear F-dependence up to $F \approx 4\ \mu J\ cm^{-2}$: this follows from the fact that the photoinduced signal normalized to F is constant in this range of excitations. At higher fluences, the amplitude shows a sub-linear fluence dependence: $\mathsf{A} \approx \sqrt{F}$.

Panel (b) shows the temperature dependence of the reflectivity transient taken at a constant excitation fluence $F = 8.4\ \mu J\ cm^{-2}$. The behaviour is identical to the early low intensity

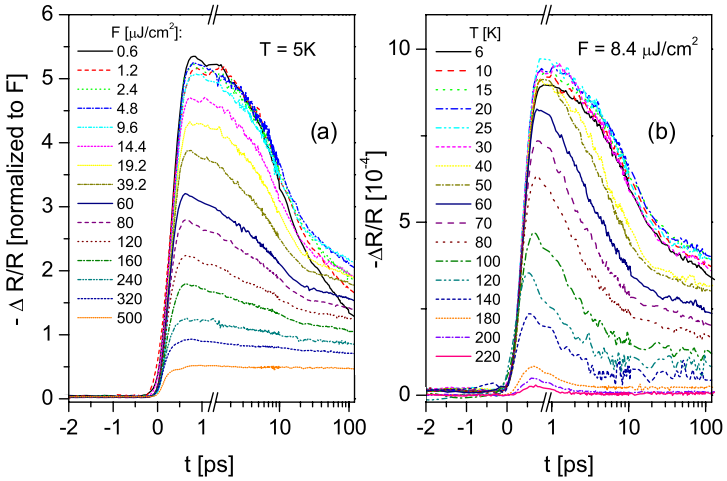

Figure 10. (a) The F-dependence of the PI reflectivity transient for the Kondo insulator SmB_6 at 5 K. The data have been normalized to F in order to emphasize the sub-linear F-dependence of the amplitude. (b) The T-dependence of the photoinduced reflectivity for $F = 8.4\ \mu\text{J cm}^{-2}$.

data [12], showing a two orders of magnitude increase in the decay rate upon warming to room temperature. Furthermore, the amplitude of the transient A also shows a pronounced temperature dependence, as observed in all heavy electron systems in the low perturbation regime configuration.

In order to test the generality of the observed excitation fluence dependence, the same experiment was performed on the Kondo insulator SmB_6. Indeed, very similar excitation fluence dependence has been observed; see figure 10.

Figure 10 presents the F- and temperature dependence of the photoinduced reflectivity of the Kondo insulator SmB_6. The behaviour is very similar to the behaviour observed for $YbAgCu_4$. The main difference is that in SmB_6 no anomalous rise-time is observed all the way to the lowest F. In addition, the fluence where A departs from a linear dependence on F is near $F \approx 12\ \mu\text{J cm}^{-2}$.

2.6. Summary of the experimental results

The main common feature of all experiments on heavy electron systems is the anomalous slowing down of the decay dynamics upon cooling. While the functional form of the relaxation dynamics was found to differ substantially between different compounds, the temperature dependence of the effective time exhibits a general trend. Figure 11(a) summarizes the temperature dependence of the decay times for the samples studied; all of the (effective) decay times were normalized to their room temperature values for presentation purposes. In addition, the amplitude of the transient was found to strongly depend on temperature, as shown in figure 11(b) for $YbAgCu_4$ and SmB_6. The observed strong temperature dependence also seems to be a quite general feature in heavy electron compounds. In addition, we should note the strong excitation fluence dependence of the photoinduced reflectivity transients, which also seems quite general.

Apart from the above, we should mention also the peculiar rise-time dynamics observed at very low temperatures in $YbAgCu_4$ and $CeCoIn_5$. It is noteworthy that the absence of the two-stage rise-time dynamics in other studied compounds could be attributed to the fact that

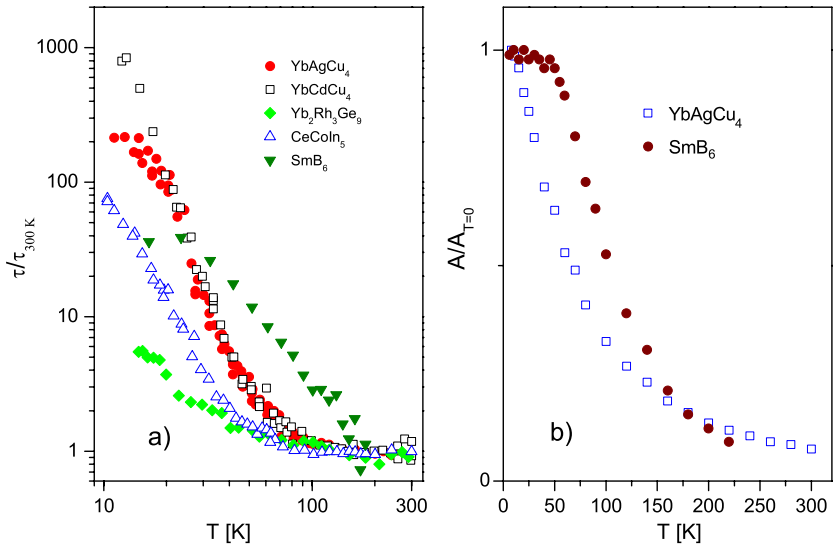

Figure 11. (a) The temperature dependence of the decay times for the heavy electron systems studied. Note that all of the decay times were normalized to their room temperature values for presentation purposes. (b) The temperature dependence of the amplitude of the photoinduced reflectivity transient for $YbAgCu_4$ and SmB_6.

their decay dynamics were found to be strongly non-exponential, and that the early time decays were substantially shorter then in $YbAgCu_4$ and $CeCoIn_5$. We should also note that $YbAgCu_4$ and $CeCoIn_5$ are the best metals of the systems studied to date.

3. Theoretical analysis

The main motivation for systematic research on carrier relaxation dynamics in these (fairly simple) heavy electron compounds, described usually by a single characteristic energy scale (Kondo temperature), was to obtain a general understanding of the phenomena. With this at hand, more complicated compounds with competing orders can be studied. One example of such compounds is $YbAg_xIn_{1-x}Cu_4$ system, where evolution from a first-order valence transition to heavy fermion behaviour [36] can be studied by means of real-time techniques [37].

Here we review the theoretical models that were developed to account for the anomalous temperature and excitation intensity dependence of the relaxation dynamics. First, we review the thermomodulation scenario, where anomalous slowing down of the relaxation was described in terms of the conventional two-temperature model (TTM). The scenario suggests that the low temperature divergence in the relaxation time generally observed in heavy electron compounds can be described by a conventional e–ph thermalization scenario, provided that there exists a mechanism of suppressed e–ph scattering when both initial and final electronic states lie within the peak in the density of states near the Fermi energy [12, 13]. Recently, an alternative model has been presented [14], where the indirect hybridization gap in the density of states (DOS) presents a bottleneck in relaxation. It was argued that in this case the relaxation phenomena can be described by the so-called Rothwarf–Taylor model [15], the model that was derived to explain the relaxation dynamics in superconductors.

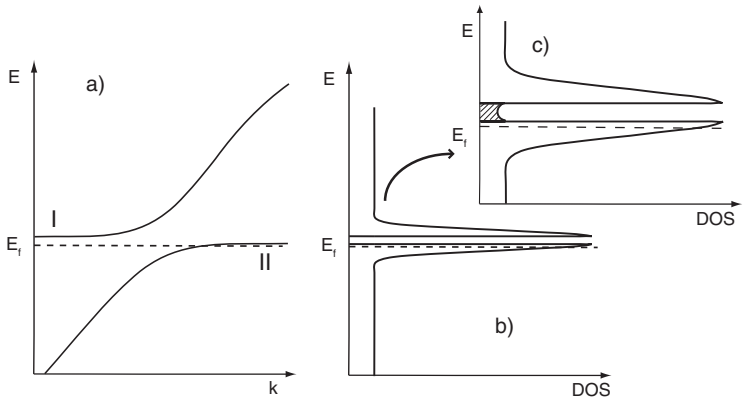

Figure 12. A generic picture of (a) the energy band dispersion and (b) the density of states (DOS) near the Fermi energy (dashed line) for a Kondo lattice or periodic Anderson model [10, 38] in the low temperature limit. (c) Detail of the hybridization gap (pseudogap). In the case of a Kondo insulator the Fermi energy lies within the hybridization gap.

To point out the principal difference between the proposed models, we plot, in figure 12, a generic band dispersion and the density of states (DOS) near the Fermi energy for the case of a periodic Anderson model [38] in the low temperature limit. Hybridization between the conduction band (with finite bandwidth) and localized f-levels leads to the band structure depicted in panel (a). In an ideal case there is a clear (indirect) gap in the density of states; see panels (b) and (c). In the case when there is a substantial amount of impurities, the gap may be partially filled. The dashed area in panel (c) presents the finite in-gap DOS in this case. In the latter case (the same is true also for the case of a clear gap if the Fermi level is far from the gap edge), the photoexcited carrier relaxation should proceed as in simple metals, the only difference being the flat band dispersion near the Fermi energy (high effective mass). The theoretical model discussed in [12, 13] can be applied in this scenario.

The alternative model assumes a well established gap E_g in the density of states, with the Fermi level within the gap (as in case of Kondo insulators) or lying close to the band edge[6] (in heavy electron metals). In the following, we are considering the case of the Kondo insulator (for simplicity); however, the same arguments can be used also for heavy fermion metals. A laser pulse excites carriers from the occupied states below E_F to the unoccupied states much higher in energy (typically 1.5 eV, the energy of photons from Ti:sapphire laser). These high energy electrons (and remaining holes) relax towards the Fermi energy by e–e and e–ph scattering and eventually reach the flat regime in the two bands. Further relaxation is suppressed due to the presence of the energy gap in the DOS; i.e. the gap in the density of states presents a relaxation bottleneck. In this scenario, after the initial (e–e and e–ph) scattering processes, which usually proceed on a sub-picosecond timescale [26], the system is characterized by excess densities of electron–hole pairs and high frequency phonons. When an electron–hole pair with energy $\geqslant E_g$ recombines, a high frequency phonon ($\omega > E_g$) is created. Since this high frequency phonons can subsequently excite electron–hole pairs, the recovery is governed by the decay of the high frequency phonon population [15]. This bottleneck in the relaxation is referred to as a phonon bottleneck [15]. Formally, the relaxation dynamics within this model are described by the phenomenological Rothwarf–Taylor model [15], which has recently been solved analytically for all limiting cases [16], enabling a comparison with the experimental data.

[6] Strictly speaking, the distance between the band edge (band II in figure 12) and the Fermi level should be considerably smaller that the size of the indirect hybridization gap E_g.

3.1. Description within the femtosecond thermomodulation scenario

The basis for the description of carrier relaxation dynamics in heavy fermions by the so-called two-temperature model [39–41] stems from the experimental observation that the relaxation times in magnetic and non-magnetic compounds were quite similar at high temperatures; see figure 3. Moreover, the relaxation dynamics of the non-HF compounds (e.g. $LuAgCu_4$) display a very weak temperature dependence, with $\Delta R/R$ recovering on a sub-picosecond timescale at all temperatures. The dynamics are similar to regular metals such as Au and Ag [26], where the recovery is governed by e–ph thermalization.

3.1.1. Femtosecond thermomodulation in normal metals. In conventional metals, the initial photoinduced change in the reflectivity arises from changes in occupation near E_F after e–e thermalization. Subsequently, the photoinduced reflectivity recovery dynamics proceed on a picosecond timescale governed by e–ph thermalization [26]. The two-temperature model (TTM) serves as a starting point in describing e–ph thermalization in metals [39–41]. It describes the time evolution of the electron (T_e) and lattice (T_l) temperatures by two coupled differential equations [26, 39]:

$$C_e(T_e)\frac{\partial T_e}{\partial t} = -g(T_e - T_l) + S(z,t) \tag{3}$$

$$C_l\frac{\partial T_l}{\partial t} = g(T_e - T_l), \tag{4}$$

where $C_e(T_e)$ and C_l are the respective heat capacities of the electrons and lattice, g $(=g(T_l))$ is the e–ph coupling function and $S(z,t)$ describes the absorbed energy, where z is the depth coordinate. Since the majority of the experiments have been performed in the low excitation intensity regime, where the estimated electronic temperature increase after photoexcitation is less than 10 K over the entire temperature range, we are considering the weak perturbation limit. In this limit (when the change in the electronic temperature is small compared to the initial temperature $T_e - T_l \ll T_l$), the relaxation of the electronic temperature is exponential with the e–ph thermalization time given by [26, 42]

$$\tau_{e-ph} = \frac{1}{g}\frac{C_eC_l}{C_e + C_l}. \tag{5}$$

Here $g(T_l)$ is in the linear response limit $(T_e - T_l \ll T_l)$ particularly simple in the case of simple metals, where the electron bandwidth is much larger then the Debye temperature Θ_D. In this case the Debye model of e–ph coupling can be used and $g(T)$ is given by $g(T) = dG(T)/dT$, where [26]

$$G(T) = 4g_\infty\left(\frac{T}{\Theta_D}\right)^5\int_0^{\Theta_D/T}\frac{x^4\,dx}{e^x - 1}. \tag{6}$$

Given that, the T-dependence of τ_{e-ph}—equation (5)—is completely determined by the e–ph coupling constant, Θ_D and $C_e(T)$. In simple metals (not heavy fermion metals) the lattice specific heat C_l is a factor 100 larger than the electronic specific heat $(C_l \gg C_e)$ over the entire temperature range in which the experiments are performed. Therefore the e–ph thermalization time τ_{e-ph} is given by

$$\tau_{e-ph} \approx \frac{C_e}{g(T_l)} = \frac{\gamma T_l}{g(T_l)}. \tag{7}$$

Here the electronic specific heat $C_e = \gamma T_l$ has been put explicitly in the model equations. For $T_l \ll \Theta_D$ the function $g(T_l)$ varies as T_l^4 while for $T_l \geqslant \Theta_D$ the function $g(T_l)$ becomes constant (g_∞). Therefore, the TTM predicts $\tau_{e-ph} \sim T_l^{-3}$ at $T_l \leqslant \Theta_D/5$ and $\tau_{e-ph} \sim T_l$

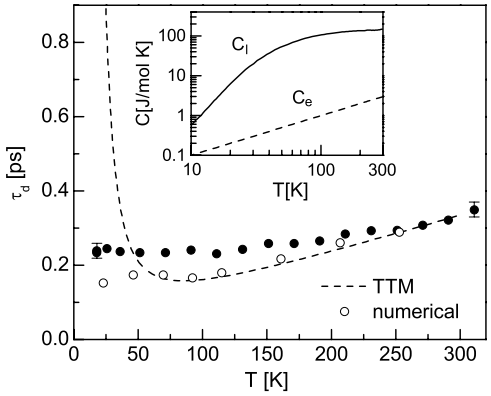

Figure 13. The temperature dependence of the decay time in $LuAgCu_4$ (solid circles) compared to the TTM simulation (dashed line). Open circles represent the result of the simulation using the coupled Boltzmann equations [13] (see text). Inset: electronic and lattice specific heat of $LuAgCu_4$.

at $T_l \geqslant \Theta_D/5$ [13]. In simple metals, g_∞ is typically 10^{17} W m^{-3} K^{-1} (e.g. for Cu $g(300\ \mathrm{K}) = 1 \times 10^{17}$ W m^{-3} K^{-1} [43]).

Figure 13 presents the results of the TTM simulation of the e–ph thermalization time as a function of temperature compared to the data on $LuAgCu_4$. The qualitative agreement between the model and the experimental data is good down to 50 K. At lower temperatures the model suggests that the decay time should increase as T^{-3}, which is not observed. In fact, the absence of the low temperature divergence of the decay time is quite general for simple metals [26, 42].

Generally, at $T > \Theta_D$, $\tau_{ep}(T)$ given by the TTM has been found to describe the temperature as well as photoexcitation intensity dependence of measured $\tau_d(T)$ [26, 43]. Moreover, since the absolute value of τ_{e-ph} is determined by *a single parameter* g_∞, the technique has been successfully used to determine the dimensionless e–ph coupling constants λ in superconductors [41, 44]. However, at low temperatures ($T \leqslant \Theta_D/5$) the TTM prediction of $\tau_{e-ph} \propto T^{-3}$ has never been observed in metals [26]; instead, at low temperatures, τ_d saturates at a constant value. The discrepancy between the experimental results and the TTM was found to be due to the fact that the TTM neglects e–e thermalization processes (by implicitly assuming that a Fermi–Dirac distribution is created instantly after photoexcitation). From simulations using coupled Boltzmann equations, it was shown [13, 26] that this discrepancy is due to the fact that at low temperatures the e–e and e–ph thermalization times are comparable. Since $\tau_{e-ph} \propto T$ above $\approx\Theta_D/5$ [26, 41], while $\tau_{e-e} \propto T^{-2}$—see equation (16) of [26]—the TTM is expected to fail at low temperatures where $\tau_{e-e} \geqslant \tau_{e-ph}$. Detailed simulations using coupled Boltzmann equations show that at high temperatures the relaxation time indeed increases linearly with temperature, as predicted by the TTM and observed experimentally (see the open circles in figure 13). At low temperatures τ_{e-ph} saturates, in agreement with the experimental data on τ_d measured for simple metals [26, 42] or non-magnetic analogues of heavy electron compounds [13].

3.1.2. Femtosecond thermomodulation in heavy electron systems. In the case of heavy electron compounds, the condition that $C_l \gg C_e$ over the entire temperature range where the experiments are performed is no longer fulfilled; see figure 14(a). In the case of $YbAgCu_4$, C_e becomes larger than C_l below 20 K.

Moreover, the density of states near the Fermi level varies strongly. Figure 14(b) shows the model DOS used to simulate the experimentally measured electronic specific heat of

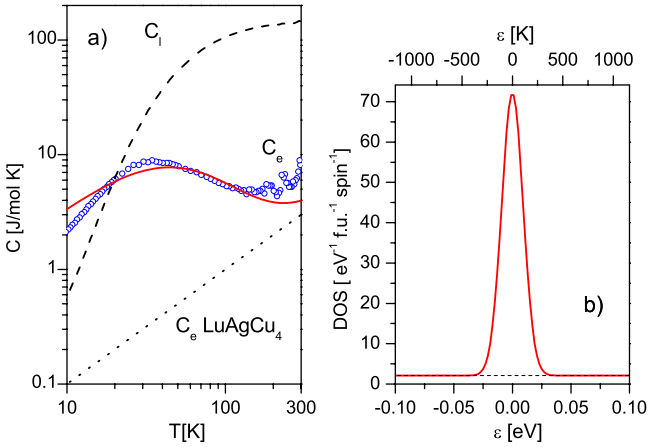

Figure 14. (a) The temperature dependence of the electronic (open circles) and lattice (dashed line) specific heats of $YbAgCu_4$. C_e for the non-magnetic $LuAgCu_4$ is plotted for comparison (dotted line). (b) The model DOS for $YbAgCu_4$ (solid line) and $LuAgCu_4$ (dashed line) used in the calculation (see text). C_e corresponding to the model DOS of $YbAgCu_4$ is plotted in panel (a) using a solid line.

$YbAgCu_4$ (solid line). For simplicity we used a simple Gaussian to represent the peak in the DOS at the Fermi level. In particular, we used $D_e(\epsilon) = D_{peak} \exp[-(\epsilon/\Delta)^2] + D_0$, where $D_{peak} = 70\,eV^{-1}$ f.u.$^{-1}$ spin^{-1}, $\Delta = 13$ meV and $D_0 = 2.1\,eV^{-1}$ f.u.$^{-1}$ spin^{-1} (D_0 is identical to the value used for $LuAgCu_4$ that gives rise to the experimental value of the Sommerfeld constant of $\gamma \sim 10$ mJ mol^{-1} K^{-2}). It reproduces the experimental T-dependence of C_e. As is evident from figure 14(b), in $YbAgCu_4$, the DOS varies strongly on the energy scale that corresponds to the temperature range of 300 K, where the experiments have been performed. Therefore, equation (6) needs to be generalized:

$$G(T) = 4g_\infty \left(\frac{T}{\Theta_D}\right)^5 \int_0^{\Theta_D/T} dx \frac{x^4}{e^x - 1} \chi(x, T). \tag{8}$$

Here $\chi(x, T)$ is included to account for the variation in the electronic DOS, $D_e(\epsilon)$, as well as to account for the possible variation of the e–ph scattering strength $F(\epsilon, \epsilon')$, over the energy range $E_F \pm \hbar\omega_D$. It can be shown, using the Fermi golden rule, that

$$\chi(x, T) = \frac{1}{\xi} \int_{-\infty}^{\infty} d\epsilon \frac{D_e(\epsilon)\, D_e(\epsilon')\, F(\epsilon, \epsilon')}{D_0^2} \{f_0(\epsilon) - f_0(\epsilon')\}, \tag{9}$$

where $\epsilon' = \epsilon + \xi$, and $\xi = xT$ and f_0 is the Fermi–Dirac distribution function. It is clear that the generalized $G(T)$ reduces to equation (6) in the case of simple metals. Namely, in metals like Au or Ag, $D_{el}(\epsilon)$ and F are approximately constant over this energy range, i.e. $D_e(\epsilon) = D_0$ and $F = 1$, giving $\chi \equiv 1$.

Figure 15 presents the result of the TTM simulation of e–ph thermalization in $YbAgCu_4$. Since $D_e(E_F)$ is almost two orders of magnitude larger than in $LuAgCu_4$, we expect that e–e thermalization is much faster in $YbAgCu_4$, and that the TTM would be valid all the way to the lowest temperatures. The calculated $\tau_{ep}(T)$ using equations (5) and (8) is plotted in figure 15(c) by the dashed line. Here the approximate $C_e(T)$ and $C_l(T)$ were used, and g_∞ was taken to be the same as for $LuAgCu_4$, while $\chi(x, T)$ was evaluated explicitly for the above $D_e(\epsilon)$ and the e–ph scattering strength was considered to be a constant, $F = 1$. It follows that in the case of an increased DOS near E_F the e–ph thermalization should proceed on a timescale much faster than

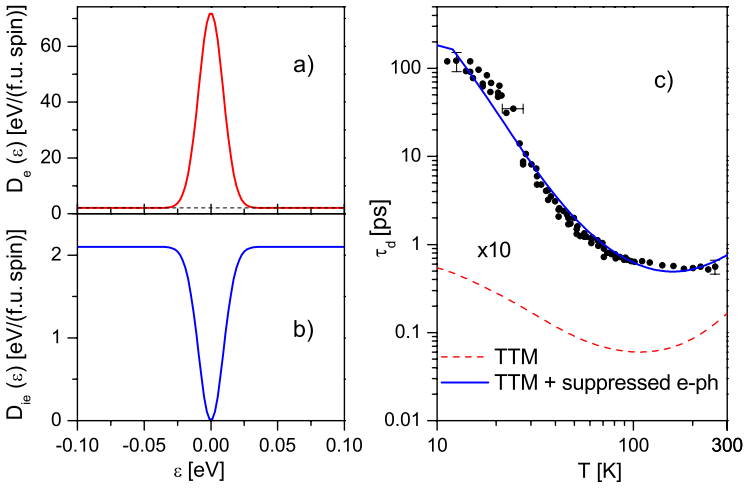

Figure 15. The TTM simulation of e–ph thermalization in $YbAgCu_4$. While panel (a) presents the model DOS used in the simulation, panel (b) presents the second part of the symmetrized function $D_e(\epsilon)D_{ie}(\epsilon') + D_e(\epsilon')D_{ie}(\epsilon) - D_{ie}(\epsilon)D_{ie}(\epsilon')$ which approximates the factor $D_e(\epsilon)D_e(\epsilon')F(\epsilon,\epsilon')$ in equation (9). This function describes the variation in $F(\epsilon,\epsilon')$ within the peak in the DOS at E_F (see text). Panel (c) shows the TTM prediction (dashed) and the simulation of the TTM with suppressed e–ph scattering when both initial and final electronic states lie within the peak in the DOS (solid line).

in simple metals, contrary to the observed temperature dependence of the decay time. Since $\tau_{e-ph}^{-1} \propto D_e$, and $D_e(E_F) \gg D_0$, the result is not surprising, implying that the simple TTM cannot account for the observed dramatic increase in τ_d at low T. We should note that neither the value of the e–ph coupling constant g_∞ nor D_0, which determine the absolute value of τ_{ep}, are necessarily the same in $YbAgCu_4$ and $LuAgCu_4$. However, even if the e–ph coupling is ten times smaller in $YbAgCu_4$ compared to $LuAgCu_4$ (which would give a ten times larger value of τ_{e-ph}, as plotted by dashed line in figure 15(c)), the observed T-dependence of τ_d still cannot be accounted for.

In order to account for the observed $\tau_d(T)$ we have considered the nature of the electronic states within the peak in the DOS, namely the hybridization of f-local moments with the conduction electrons. The hypothesis has been put forward that the e–ph scattering within the DOS peak is suppressed, since the band dispersion near E_F (see figure 12) is much weaker than in regular metals. In fact, it seems plausible that the situation when the Fermi velocity v_F is smaller than the sound velocity v_s can be realized in these systems. Should this be realized, *momentum and energy conservation* prohibits e–ph scattering when both initial and final electron states lie within the energy range where $v_F < v_s$. This is depicted in figure 16.

A rough estimate shows that the situation of $v_F < v_s$ could be realized in $YbAgCu_4$. Assuming a parabolic band with $E_F \sim T_K \sim 100$ K, and 0.85 carriers per formula unit [45], one obtains $v_F \sim 4$ km s^{-1}, while the longitudinal sound velocity for $YbIn_{1-x}Ag_xCu_4$ ($x < 0.3$) is $\approx$4.4 km s^{-1} along the [111] direction [46] (similar v_s is expected for $YbAgCu_4$). Even though a parabolic dispersion relation is just a rough approximation, and a direct measurement such as the de Haas–van Alphen effect is required to obtain v_F, this simple estimate supports this idea.

The applicability of this particular e–ph scattering suppression mechanism has some limitations. The model assumes that the e–ph thermalization proceeds via scattering of electrons with acoustic phonons only. Therefore, this mechanism is operational only at temperatures when k_BT and Δ are lower than the first optical phonon energy. Since the first

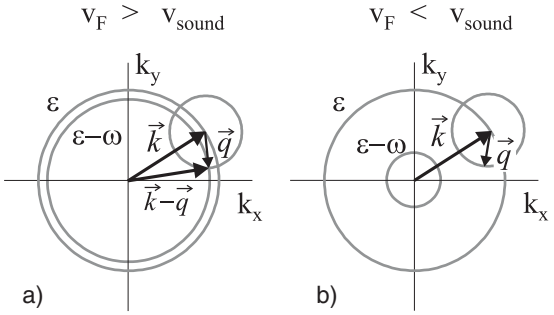

Figure 16. Schematic demonstration of suppressed e–ph scattering for the case of $v_F < v_s$. In the normal case (when $v_F > v_s$), illustrated in panel (a), there are plenty of possible e–ph scattering processes where the electron scatters from a state with an energy ε to a state with an energy $\varepsilon - \omega$ by emitting a phonon with energy ω. Note that for an acoustic phonon $\omega = v_s q$, where q is the phonon wavevector. (b) In the case when $v_F < v_s$, however, the electron dispersion is weaker that the phonon dispersion. Therefore, the distance between the spheres with energies ε and $\epsilon - \omega$ is larger than ω corresponding to the momentum $\vec{q} = \vec{k} - \vec{k}'$. Therefore, this process is prohibited by the momentum and energy conservation law.

optical phonon energies in these compounds are at about 100 cm^{-1}, while the temperature range of interest is usually below 100 K, this limitation should not be critical for applicability of the model.

On the other hand, strong impurity scattering may also limit the applicability of the e–ph scattering suppression model. Impurity scattering results in the effective uncertainty in the electron energy, $\Delta E \approx \hbar/\tau$, where τ^{-1} is the impurity scattering rate. Therefore, one would expect that below some characteristic temperature T^*, when ΔE becomes comparable to the transferred energy in the e–ph scattering process, the e–ph energy and momentum scattering constraint would become ineffective. The average energy transferred during the e–ph scattering event is proportional to the temperature, therefore in the limit of $v_s \gg v_F$ the temperature below which the e–ph scattering suppression model is expected to fail is $k_B T^* \approx \hbar/\tau$. The impurity scattering rate τ^{-1} can be estimated from the low temperature conductivity data using the Drude formula $\tau = 4\pi\sigma/\omega_p^2$, where σ is the DC conductivity and ω_p the plasma frequency. In $YbAgCu_4$ the renormalized plasma frequency is approximately 0.35 eV [47], while $\sigma^{-1} \approx 6\ \mu\Omega$ cm [25], giving $\tau \approx 6$ ps (corresponding to the electron mean free path $l \approx 250$ Å). It follows that in $YbAgCu_4$ $T^* \approx 2$ K (in the limit $v_s \gg v_F$), suggesting that the impurity scattering is not the limiting factor in applicability of this particular e–ph scattering suppression mechanism. We should note that similar numbers for the low temperature mean free path are obtained also for other heavy electron systems [48].

Using the hypothesis that e–ph scattering is suppressed in the vicinity of the Fermi level, good agreement with the experimental data can be obtained; see figure 15(c). Here it was assumed (for simplicity) that the e–ph interaction strength $F(\epsilon, \epsilon')$ entering equation (9) smoothly vanishes as ϵ and $\epsilon' \to E_F$. The variation of $F(\epsilon, \epsilon')$ is implemented into the TTM simulation by approximating the factor $D_e(\epsilon)D_e(\epsilon')F(\epsilon, \epsilon')$ in equation (9) with the symmetrized function $(D_e(\epsilon)D_{ie}(\epsilon') + D_e(\epsilon')D_{ie}(\epsilon) - D_{ie}(\epsilon)D_{ie}(\epsilon'))$, where $D_{ie}(\epsilon) = D_0 - D_0 \exp[-(\epsilon/\Delta')^2]$. The resulting $\tau_{e-ph}(T)$, using $\Delta' = 24$ meV, and $g_\infty = 4.5 \times 10^{14}$ W mol^{-1} K^{-1} is plotted by the solid line in figure 15(c). Indeed, extremely good agreement with the data is obtained, even though τ_d spans more than two orders of magnitude.

With the hypothesis that e–ph scattering is suppressed within the DOS peak, the experimental observation of anomalous T-dependence of τ_d can be understood. Namely,

at $T < T_K$, $C_e(T)$ increases dramatically compared to normal metals. On the other hand e–ph thermalization becomes more and more difficult as the temperature is lowered since most of the electron relaxation should occur within the DOS peak, where the e–ph scattering is blocked by *energy and momentum* conservation. Therefore, the thermalization between electrons and the lattice occurs very slowly, giving rise to the divergent τ_{e-ph} on approaching 0 K. The simulations assume a temperature independent peak in the DOS, assuming that many-body and correlation effects can be described by the effective, temperature independent model parameters. This may be an oversimplification of the physics of heavy fermion systems. However, the relaxation time simulations and specific heat calculations of this phenomenological model depend only weakly on a T-dependent DOS, as long as the peak width in the DOS does not vary faster than the temperature. While this model explains the main features of the data, i.e. the low-T divergence of τ_{e-ph}, the anomalous temperature dependence of the rise-time dynamics in $YbAgCu_4$ remains unexplained.

3.1.3. Amplitude of the transient within the TTM scenario. As shown above, the amplitude of the photoinduced reflectivity transient is in heavy electron systems found to be strongly temperature and excitation fluence dependent. This observation was not discussed in the first report [12]. To check whether these observations can also be accounted for by the femtosecond thermomodulation scenario, we consider the model introduced recently by Hase *et al* [42], which discusses the amplitude of the transient within the TTM scenario. We should note that the additional e–ph scattering suppression mechanism had to be introduced in order to account for the recovery dynamics data; when considering the amplitude of the photoinduced absorption no additional constraint is required. In other words, heavy electron systems can be treated as simple metals (with varying DOS near the Fermi level). Moreover, since the DOS near E_F is considerably higher in heavy electron systems than in simple metals, and the e–e thermalization rate is proportional to $D_e(\epsilon)^3$, the assumption of electrons being thermalized within 100 fs after photoexcitation should be valid throughout the temperature range of interest.

The main idea of the model is that the changes in the reflectivity at optical frequencies (e.g. 1.5 eV) are due to photoinduced absorption, with photoinduced quasiparticles (in the energy range of $k_B T_e$ around the Fermi energy) as initial states and with final states well above/below the Fermi energy [27, 49]. The idea is based on the fact that the initial e–e thermalization proceeds on the sub-100 fs timescale; therefore photoexcited carriers reach the states near the Fermi level in a time comparable to the experimental resolution. Therefore, using the Fermi golden rule, the amplitude of the transient (photoinduced absorption) is proportional to the change in the occupied electronic density of states near E_F, i.e. the amplitude of the photoinduced transient should be proportional to the photoinduced quasiparticle density, n_p. Considering that within 100 fs after excitation the electron system is already thermalized at an elevated temperature T_e', the amplitude A is given by the difference in the densities of electron–hole pairs n before and after photoexcitation

$$\mathsf{A} \propto n_p = n_{T_e'} - n_{T_e} = \int_0^\infty \mathrm{d}\epsilon D_e(\epsilon) \left[f_0\left(\epsilon, T_e'\right) - f_0\left(\epsilon, T_e\right) \right], \tag{10}$$

where $f_0(\epsilon, T)$ is the Fermi–Dirac distribution function at temperature T, while $D_e(\epsilon)$ is the electron density of states.

Simple metals. Let us first consider the case of simple metals. In the limit when the temperature is much lower than the Fermi energy, which is the case realized in most situations, and $D_e(\epsilon)$ is constant near the Fermi level, the number density of the electron–hole pairs n is, in a Landau Fermi liquid, exactly proportional to the (electronic) temperature, $n_{T_e} \propto T_e$.

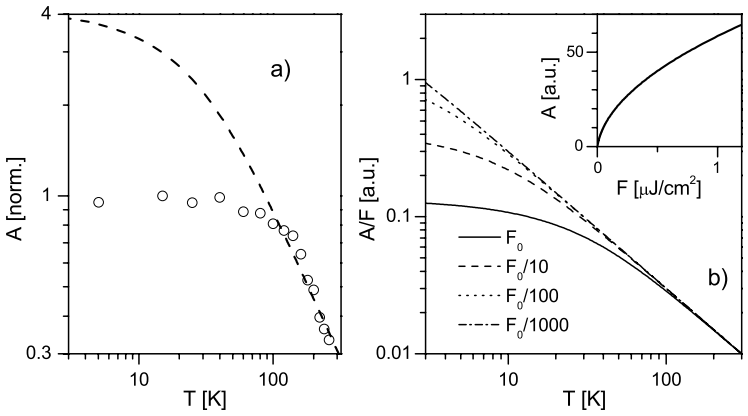

Figure 17. (a) The temperature dependence of the transient amplitude A for $LuAgCu_4$ (open circles) together with the TTM prediction, equation (12) (dashed line). (b) The TTM simulation of the temperature and excitation fluence F dependence of the amplitude A in $LuAgCu_4$ ($F_0 = 1\ \mu J\ cm^{-2}$). The amplitude is normalized to the fluence to emphasize the nonlinear behaviour at low temperatures. Inset to (b): the predicted low temperature F-dependence of A. The simulation considers $LuAgCu_4$ at 10 K.

Under the assumption that after photoexcitation all the absorbed energy initially goes into the electronic subsystem, and that electrons are thermalized (in a time comparable to the time resolution) at an elevated electronic temperature T_e' (adiabatic approximation), it follows from equation (10) that the amplitude of the transient A is

$$\mathsf{A} \propto n_p = n_{T_e'} - n_{T_e} \propto T_e' - T_e. \tag{11}$$

For simple metals, the electronic specific heat is $C_e = \gamma T_e$, where γ is the Sommerfeld coefficient which is constant up to temperatures comparable to the Fermi temperature. Using the energy conservation law $U_l = \int_{T_0}^{T_0+\Delta T} \gamma T_e \, dT_e$, where U_l is the absorbed energy density, equation (11) simplifies to

$$\mathsf{A} \propto T_e' - T_e = \sqrt{T_e^2 + 2U_l/\gamma} - T_e. \tag{12}$$

There are several important implications of equation (12). First of all, the amplitude of the transient is maximum at low temperatures, and decreases as the temperature is increased. Second, at low temperatures ($T_e < \sqrt{2U_l/\gamma}$) a sub-linear excitation intensity dependence of the transient is expected, while at high temperatures ($T_e \gg \sqrt{2U_l/\gamma}$) the dependence becomes linear.

To compare the TTM prediction with the experimental data, the excitation energy density needs to be determined. In the low excitation density experimental configuration the maximum excitation fluence, F, is of the order of 1 $\mu J\ cm^{-2}$. Taking into account that the optical penetration depth in these materials in of the order of 15 nm, and a reflectivity of about 70% (see footnote 3), the absorbed energy density is in the range of $U_l < 0.2\ J\ cm^{-3}$. For reference, at 10 K the transient electronic temperature increase in $LuAgCu_4$ is 55 K at $F = 1\ \mu J\ cm^{-2}$.

The temperature dependence of the amplitude A in $LuAgCu_4$ is plotted in figure 17(a). It can be well fitted by equation (12) down to ≈80 K. At lower temperatures A nearly saturates, while the TTM predicts a further increase in amplitude. In fact a similar observation was recently reported in Zn [42], in which it was argued that at low temperatures the TTM fails and that electrons are still non-thermal on this timescale. Figure 17(b) shows the predicted excitation fluence dependence of the transient in $LuAgCu_4$ ($\gamma \approx 50\ \mu J\ cm^{-3}\ K^{-2}$). It follows

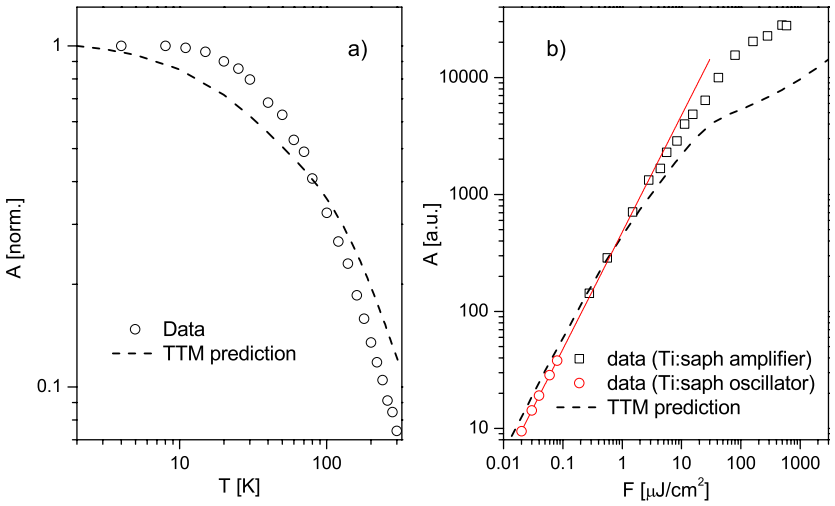

Figure 18. (a) The temperature dependence of amplitude A in $YbAgCu_4$ (open circles), compared to the prediction on the TTM (dashed line). (b) The photoexcitation intensity (F) dependence of A in $YbAgCu_4$ (open symbols) compared to the TTM simulation (dashed). Open squares represent the data taken with the low repetition rate amplifier, while open circles represent the data obtained with the high repetition rate Ti:sapphire oscillator, where $A \propto F$ was found over the entire range. The solid line is a linear fit at low F.

that the sub-linear intensity dependence could only be observed below ≈30 K in this range of excitation densities. Experimentally, the sub-linear excitation dependence of amplitude was not observed in $LuAgCu_4$ in this range of excitations. A similar lack of sub-linear dependence of amplitude at low temperatures was also reported in Zn [42], and attributed to the general failure of the TTM at low temperatures.

Heavy fermion metals. In heavy fermion metals, the Sommerfeld coefficient γ is not constant over the temperature range of interest. In fact, linear dependence of C_e versus temperature is observed only at very low temperatures; see figure 14(a). Therefore, in order to study the prediction of the TTM for the temperature and excitation intensity dependence of the amplitude A, equation (10) has to be evaluated numerically for each initial temperature and excitation level. To do that, one first needs to calculate the corresponding increase in the electronic temperature following photoexcitation. This can be easily done via $U_l = \int_{T_0}^{T_0+\Delta T} C_e(T)\,dT$, providing that the data on the temperature dependence of the electronic specific heat, as well as the material's optical properties, are available.

To simulate the expected temperature and excitation fluence dependence of the photoinduced carrier density ($A \propto n_{pe}$) in the heavy fermion metal $YbAgCu_4$ we used the model DOS to approximate the experimentally measured $C_e(T)$; i.e. $D_e(\epsilon) = D_{peak}\exp[-(\epsilon/\Delta)^2] + D_0$ ($D_{peak} = 70$ eV^{-1} f.u.$^{-1}$ spin^{-1}, $\Delta = 13$ meV and $D_0 = 2.1$ eV^{-1} f.u.$^{-1}$ spin^{-1}. Furthermore, to determine the absorbed energy density U_l, required to determine the increase in the electronic temperature after excitation, $\Delta T = T_e' - T_e$, we have used an optical penetration depth of 15 nm and reflectivity of 0.7 (see footnote 3). From this calculated temperature increase, the amplitude of the transient is calculated using equation (10) where the same model DOS was used. For reference, at 10 K the transient electronic temperature increase in $YbAgCu_4$ is ≈9 K for $F = 1$ μJ cm^{-2}.

The result of the simulation of the predicted temperature and excitation dependence of the transient in $YbAgCu_4$ within the TTM is plotted in figure 18, along with the experimental data.

The agreement between the two temperature dependences is merely qualitative. For example, the predicted amplitude A at low temperatures decreases faster upon warming than the experimental data, while at high temperatures the signal amplitude decreases faster than theoretical, so at 300 K the two are almost a factor of two different. In addition, there is a general observation that is difficult to account for within the TTM model; namely the plateau in the temperature dependence of amplitude observed at low temperatures. While the plateau is clearly present in $YbAgCu_4$ it is even more pronounced in $YbCdCu_4$ or SmB_6. Due to the uncertainty in the optical properties used to estimate the excitation energy density, we estimate that an absolute value of U_l is only known to within a factor of two. Thus, we have performed the simulations also for a factor of two higher and lower excitation densities, but the agreement between the experimental and theoretical temperature dependences of A is not substantially improved from the one plotted in figure 18 (for the data taken at $F = 8.4\ \mu J\ cm^{-2}$).

Figure 18(b) shows the simulated excitation intensity dependence of amplitude (dashed line) taken at low temperatures (5 K) compared to the data extracted from figure 9 (open squares). Experimental data show linear $A \propto F$ dependence up to $\approx 4\ \mu J\ cm^{-2}$, after which the dependence becomes sub-linear. Theoretical simulations within the TTM model also show similar behaviour; however, the crossover intensity, where sub-linear behaviour becomes evident, occurs at about $0.3\ \mu J\ cm^{-2}$, more than an order of magnitude lower than the experimental value. While there can be up to a factor of two uncertainty in the absolute value of the experimental excitation energy density (e.g. due to the uncertainty in determination of the absolute excitation level density), it is hard to imagine an order of magnitude correction. In addition, the model will have a hard time explaining the clear saturation of amplitude observed in SmB_6; see section 3.2.1.

Overall, the agreement between the experimental data and the TTM simulation of the temperature and excitation intensity dependence of amplitude is qualitative. The quantitative analysis, on the other hand, shows substantial discrepancies; for example, the crossover from linear to sub-linear excitation intensity dependence is obtained in the theoretical simulation at an excitation density which is an order of magnitude lower than the experimental one. On the other hand, there are some approximations made in the analysis (the shape and the position of the peak in the density of states), which may not perfectly reflect the real low energy electronic structure in these materials.

3.2. Hybridization gap—phonon bottleneck scenario

As pointed out above, there are several observations that cannot be accounted for by the thermomodulation scenario. The anomalous rise-time dynamics observed at low temperatures in some heavy fermion compounds are clearly the observation that is the most difficult to explain with the TTM. Furthermore, the strongly nonlinear dependence of the relaxation rate and amplitude, as well as the temperature dependence of amplitude, is also not in very good agreement with the TTM.

On the other hand, similar temperature and excitation intensity dependence of the rise-rime dynamics has also been observed in superconductors [3]. Moreover, the temperature dependence of the relaxation rate observed in heavy electron systems also closely resembles the data in both conventional [3] and cuprate [50, 51] superconductors. In superconductors, the photoexcited carrier dynamics are governed by the presence of the superconducting energy gap in the density of states. The very similar behaviour of the photoexcited carrier dynamics in superconductors and heavy electron systems suggests that the processes governing the relaxation dynamics in heavy electron compounds (both Kondo insulators and heavy fermion metals) may be the same as in superconductors, governed by the presence of a narrow gap

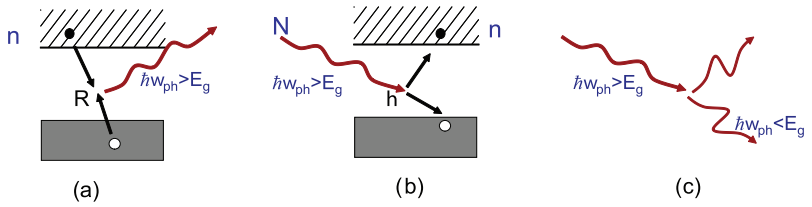

Figure 19. Schematic diagram of the relaxation processes in photoexcited narrow band semiconductors: (a) electron–hole recombination with creation of a high frequency phonon, (b) creation of an electron–hole pair via high frequency phonon absorption, (c) anharmonic decay of high frequency phonon.

in the density of states. Indeed, if hybridization of the local f-moments with conduction electrons leads to the opening of a well established (indirect) hybridization gap (E_g) near E_F, see figure 12, a similar relaxation bottleneck is expected as observed in superconductors [16]. The analogy with superconductors is straightforward for the case of Kondo insulators, where E_F lies within the gap [34]. However, the same bottleneck physics [16] is expected to be effective even in the case of metallic heavy fermions, if E_F lies close to the hybridization gap edge (if the distance between the gap edge and $E_F \ll E_g$).

Relaxation phenomena for nonequilibrium superconductors have revealed some of the most intriguing problems in condensed matter physics since the 1960s [52]. The presence of the superconducting gap in the single particle excitation spectrum was found to present a relaxation bottleneck for photoexcited carrier relaxation [3]. The minimal model that describes the relaxation of the (photo)excited superconductor was formulated in 1967 by Rothwarf and Taylor [15]. Pointing out that the phonon channel should be considered when discussing relaxation processes, they described the relaxation dynamics by a set of two coupled nonlinear-differential equations [15]. While in the low perturbation limit the equations can be linearized [53], it was shown only recently that approximate analytical solutions can be obtained for all limiting cases [16]. Analytical solutions enable comparison of the experimental data with the model, and have revealed that the Rothwarf–Taylor (RT) model can account for both the rise-time dynamics [3], as well as the superconducting state recovery as a function of excitation fluence (F) and T [16].

Before analysing the F- and T-dependence of the PI reflectivity transients, we briefly review the RT model and its solutions, using language appropriate for a photoexcited, narrow gap semiconductor; see figure 19. Following photoexcitation, high energy electrons initially release their energy via e–e and e–ph scattering. Following this process, which usually proceeds on a sub-picosecond timescale [26], the system is characterized by excess densities of electron–hole pairs (EHPs) and high frequency phonons (HFPs). When an EHP with an energy $\geqslant E_g$ (E_g is the gap) recombines, a high frequency phonon ($\omega > E_g$) is created. Since HFPs can subsequently excite EHPs, the recovery is governed by the decay of the HFP population [15]. The dynamics of the EHP and HFP populations are determined by [15]

$$\mathrm{d}n/\mathrm{d}t = \eta N - Rn^2 \tag{13}$$

$$\mathrm{d}N/\mathrm{d}t = -\eta N/2 + Rn^2/2 - \gamma(N - N_T). \tag{14}$$

Here n and N are the concentrations of EHPs and HFPs, respectively, η is the probability for EHP creation by HFP absorption, and R the rate of electron–hole recombination with the creation of an HFP. N_T is the concentration of HFPs in thermal equilibrium, and γ their decay rate (governed either by anharmonic decay or by diffusion out of the excitation volume).

The thermal equilibrium concentrations of HFPs and EHPs (n_T) satisfy the detailed balance equation $Rn_T^2 = \eta N_T$. Depending on the initial conditions (n_0 and N_0, which are concentrations of EHPs and HFPs after photoexcitation and the initial e–e and e–ph avalanche process) and the ratio of γ/η, several different regimes can be realized [16]. It follows from the RT analysis that the picosecond rise-time dynamics are observed at low F and temperature, when the combined photoexcitation and initial avalanche processes lead to an excess phonon population with respect to the detailed balance condition; i.e. $Rn_0^2 < \eta N_0$ [16]. This is in turn followed by the 'thermalization' of the EHP and HFP distributions leading to quasi-stationary distributions of n_s and N_s that satisfy [3, 16]

$$Rn_s^2 = \eta N_s \tag{15}$$

$$n_s = \frac{R}{4\eta}\left(\sqrt{1 + \frac{16R}{\eta}n_0 + \frac{8R}{\eta}N_0} - 1\right). \tag{16}$$

Since the photoinduced reflectivity change (due to photoinduced absorption) is proportional to the photoexcited carrier density, the resulting photoinduced reflectivity shows an initial fast rise-time ($n(t)$ reaches n_0) followed by a picosecond rise where $n(t)$ reaches n_s. These picosecond rise-time dynamics should depend on both the initial temperature and excitation level as observed both in MgB_2 superconductor [3] and $YbAgCu_4$; see figures 2(a) and 9(b). The recovery proceeds on a much longer timescale and is governed by HFP decay.

There are several important predictions of the model that can be used to determine whether the photoexcited carrier dynamics in heavy electron systems indeed follow the Rothwarf–Taylor kinetics.

3.2.1. Temperature and F-dependence of the transient amplitude. The amplitude of the transient is again assumed to be proportional to the photoexcited electron–hole density; i.e. $\mathsf{A} \propto n_s - n_T$, where n_s is given by equation (16). The density of thermally excited electron–hole pairs, n_T, in a narrow band semiconductor is given by

$$n_T \simeq T^p \exp(-E_g/2T). \tag{17}$$

Here p is a parameter of the order of 1, which depends on the exact shape of the density of states near the gap edge. For the hybridization gap scenario, the shape of the DOS should be close to that of a BCS superconductor, where p is exactly $1/2$.

At low enough temperatures, the number of thermally excited carriers is strongly suppressed, and $\mathsf{A} \propto n_s$. Furthermore, since n_0 and N_0 are, at low T, proportional to F, it follows from equation (16) that $\mathsf{A} \propto \sqrt{1 + cF} - 1$, where c is a constant. This implies that the amplitude A should be strongly F-dependent at low temperatures, as observed; see figure 20.

As seen in figure 20 the F-dependences of A for both SmB_6 and $YbAgCu_4$ are in excellent agreement with the prediction of the RT model. At high fluences, though, the amplitude is found to saturate, especially in SmB_6. This kind of behaviour is not too surprising in the systems under investigation, since strong photoexcitation may lead to a smearing of the gap structure, or even some type of photoinduced phase transition.

Taking into account that $\mathsf{A} \propto n_s - n_T$, and with n_s given by equation (16), it can be shown that the temperature dependence of A is entirely governed by the temperature dependence of the density of thermally excited electron–hole pairs, n_T. Specifically, it was shown that $n_T(T)$ can be extracted directly from the measurement of the temperature dependence of the amplitude A. In particular, it follows that [16]

$$n_T(T) \propto \mathcal{A}^{-1} - 1, \tag{18}$$

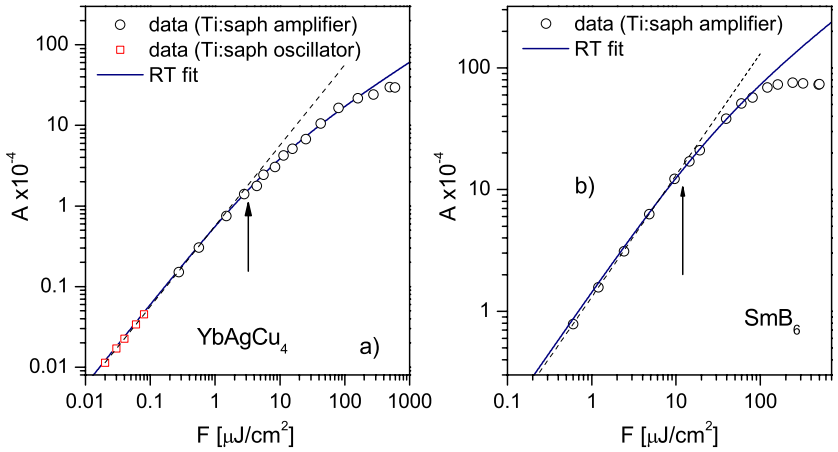

Figure 20. Photoexcitation fluence dependence of the amplitude A on (a) $YbAgCu_4$ and (b) SmB_6 taken at the base temperature of 5 K. The solid lines are the predicted dependences for the Rothwarf–Taylor bottleneck model, while the dashed lines represent a linear fit to the low excitation intensity data. The arrows indicate the departure from $A \propto F$ dependence.

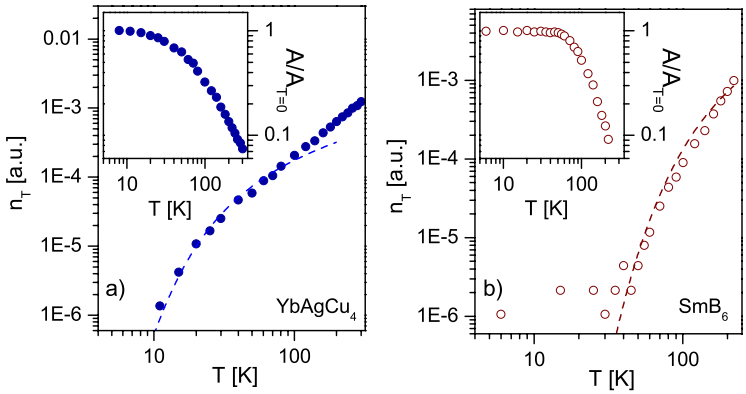

Figure 21. The temperature dependence of the density of thermally excited electron–hole pairs, n_T, extracted from the temperature dependence of A (plotted in insets) for (a) $YbAgCu_4$ and (b) SmB_6. The dashed lines represent the best fit with equation (17), giving the values of the hybridization gap E_g of 100 and 550 K for $YbAgCu_4$ and SmB_6, respectively.

where $\mathcal{A}(T)$ is the normalized amplitude (normalized to its low temperature value, $\mathcal{A}(T) = \mathsf{A}(T)/\mathsf{A}(T \longrightarrow 0)$). The importance of this relation lies in the fact that the temperature dependence of $n_T(T)$ is governed by the temperature dependence and the magnitude of the gap in the DOS; see equation (17). Therefore, an analysis of $\mathsf{A}(T)$ enables one to extract the value of the energy gap.

In figure 21, we plot the temperature dependence of n_T for $YbAgCu_4$ and SmB_6. In both data sets n_T changes by almost three orders of magnitude between 20 and 200 K. Furthermore, the absence of any discontinuity or change of slope of n_T at high temperatures suggests that the hybridization gap structure persists to high temperatures, as observed, for example, in the photoemission spectroscopy of Kondo insulators [54]. Therefore, we consider the hybridization gap to be present at all T, and to a first approximation, to be temperature independent.

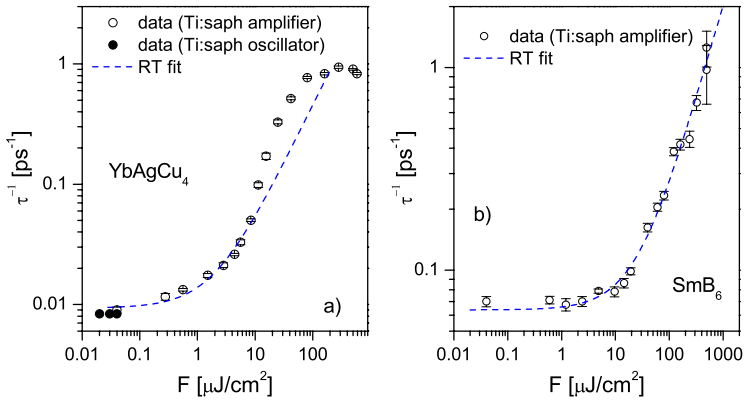

Figure 22. The excitation density dependence of the initial relaxation rate τ^{-1} for (a) $YbAgCu_4$ and (b) SmB_6 at 5 K. The dashed lines are fits to the data with the RT model, $\tau^{-1} \propto (n_s + n_T)$ (see text).

Furthermore, we assume a BCS-like DOS near the gap edge, i.e. $p = 0.5$. Fitting n_T with equation (17), we find, for SmB_6, an excellent agreement over the entire temperature range with $E_g \approx 550$ K. In $YbAgCu_4$, on the other hand, the agreement is good up to ≈120 K, with the extracted value of $E_g \approx 100$ K. At higher temperatures in $YbAgCu_4$, n_T starts to increase faster, possibly due to a partial suppression of the gap at high temperatures.

3.2.2. Temperature and F-dependence of the relaxation rate. The initial relaxation rate τ^{-1} is in the RT model given by [16]

$$\tau^{-1} = \frac{2R\gamma(n_s + n_T)}{\eta^2(1 + 2\gamma/\eta)}. \tag{19}$$

This suggests that at low excitation levels (or when the temperature is high), where $n_s \approx n_T$, the relaxation rate should be independent of the excitation level. On the other hand, at low temperatures and considerable fluences, τ^{-1} is expected to increase linearly with F.

As shown in figure 22, the data for SmB_6 agree well with the model over the entire range of F. In $YbAgCu_4$, on the other hand, at high F the experimental rate increases faster than the theoretical prediction, finally saturating at densities above 100 μJ cm^{-2}.

It is easy to demonstrate that the temperature dependence of τ^{-1} is governed by the T-dependence of n_T as well. Assuming R, γ, and η to be temperature independent[7], equation (19) can be rewritten as $\tau^{-1}(T) = \Gamma[(n_s - n_T) + 2n_T]$, where Γ is a proportionality constant. Since $n_s - n_T$ is decreasing with increasing temperature at a rate much slower than τ^{-1} is increasing (see figure 11), the dominant term responsible for the temperature dependence of τ^{-1} is the second term in equation (20). Moreover, in the case when excitation fluence is constant, the temperature dependence of $n_s - n_T$ is also entirely governed by the temperature dependence of n_T. Since $A \propto n_s - n_T$ and $n_T \propto \mathcal{A}^{-1} - 1$, it follows that

$$\tau^{-1}(T) = \Gamma[\delta(\varepsilon n_T + 1)^{-1} + 2n_T]. \tag{20}$$

Here δ and ε are constants that depend only on the photoexcitation intensity. Hence, for constant F, $\tau^{-1}(T)$ is entirely determined by the T-dependence of n_T.

[7] Note that this is a good approximation in the case when the gap closes in the mean field-like fashion, i.e. $E_g \to 0$ as $T \to T_c$, where T_c is a mean field critical temperature, then at temperatures near the critical temperature $\gamma(T) \propto E_g(T)$. This leads to a divergence of τ as $T \to T_c$, as discussed in [2].

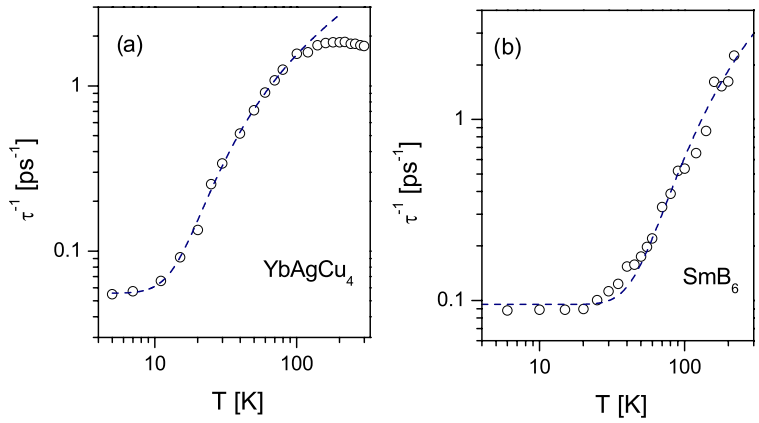

Figure 23. The temperature dependence of the initial relaxation rate, τ^{-1}, for (a) $YbAgCu_4$ and (b) SmB_6 for $F = 8.4\ \mu J\ cm^{-2}$. The dashed lines are fits to the data with equation (20). The extracted values of the indirect hybridization gap E_g were 85 and 350 K, for $YbAgCu_4$ and SmB_6, respectively.

The temperature dependences of τ^{-1} on $YbAgCu_4$ and SmB_6 are shown in figure 23. In both cases, the relaxation rate saturates at low temperatures, and then increases by nearly two orders of magnitude upon warming to room temperature. In SmB_6, τ^{-1} increases all the way to the highest temperatures measured, while in $YbAgCu_4$, τ^{-1} saturates above $\approx$160 K.

It is straightforward to show that there is qualitative agreement between the relaxation rate data and the model described by equation (19). At intermediate temperatures, $n_s - n_T \ll n_T$, and τ^{-1} is governed by the T-dependence of n_T exhibiting $\exp(-E_g/2T)$ behaviour. At low enough T, however, $n_s \gg n_T$ and the relaxation time saturates, as observed. We fit the $\tau^{-1}(T)$ data with equation (20) and find remarkable agreement. The extracted values of the gap are $E_g \approx 85$ K for $YbAgCu_4$ and $E_g \approx 350$ K for SmB_6, somewhat lower than the values extracted from the fit to n_T. This can be partially attributed to the fact that the T-dependence of R, γ, and η was neglected, as well as to microscopic details, such as potential gap anisotropy.

A comparison with the literature shows that for SmB_6 there is a large spread of published values for E_g [55]; however, our estimate is in close agreement with the T-independent pseudogap energy scale of 290 cm^{-1} (450 K) from a recent Raman scattering study [55]. The value of $E_g \approx 100$ K for $YbAgCu_4$ is also in close agreement with recent optical data [21].

The overall agreement and self-consistency of the data with the prediction of the Rothwarf–Taylor model clearly presents a strong argument that the relaxation kinetics in heavy electron systems are indeed governed by the presence of a weakly temperature dependent hybridization gap [10, 54].

3.3. Summary

The overall agreement and self-consistency of the data with the Rothwarf–Taylor model clearly presents a strong argument that relaxation kinetics in heavy electron systems are indeed governed by the presence of a weakly temperature dependent hybridization gap [10, 54]. This hypothesis is further supported by the close similarity between the observed carrier relaxation dynamics in heavy electron compounds and other systems with a narrow gap in the density of states, like superconductors and charge density wave systems. Finally, the data on the temperature dependences of both the amplitude and relaxation rate can be quantitatively explained by this model with a single fitting parameter: the magnitude (and the temperature

dependence) of the indirect hybridization gap. The extracted values of the gap are found to be in close agreement with the published values determined by more conventional spectroscopic techniques.

4. Summary and conclusions

In this paper, we have reviewed experiments on the photoexcited carrier relaxation dynamics in heavy electron systems and presented the current state of understanding of the relaxation phenomena in this class of materials. We have studied several heavy electron compounds (both metallic and insulating), with different crystal structures and with different low temperature properties. The main observation of the slowing down of relaxation upon cooling, where the relaxation time decreases by more than three orders of magnitude between room temperature and liquid helium temperature, seems quite general.

The fact that this observation is so general is quite striking. It is observed in both metallic [12] and insulating [14] compounds. In addition, we have found that the temperature dependence is also unaffected by the conduction band carrier density. As an example, we can compare $YbAgCu_4$ and $YbCdCu_4$. Their thermodynamic properties can both be well described within the single-impurity model [10, 11], both having very similar Kondo energy scales. On the other hand, the residual resistivity in $YbCdCu_4$ is an order of magnitude higher than that in $YbAgCu_4$, implying a much lower conduction band carrier density [25]. Comparison of the photoinduced carrier dynamics data, see figure 5, reveals extremely close agreement between the two, suggesting that the conduction band carrier density does not play a major role. We should note, however, that it follows from the systematics that in better metals the distribution of relaxation rates is generally narrower, i.e. the relaxation is closer to a single exponential.

A similar temperature dependence of the relaxation rate was found in $Yb_2Rh_3Ga_9$, where crystal field splitting effects dominate the low temperature physical properties (the crystal field splitting in $Yb_2Rh_3Ga_9$ is larger than the Kondo temperature [29]). Finally, similar results were also obtained in the heavy fermion $CeCoIn_5$, which appears to display strong intersite coupling [32].

In order to further elucidate on the physics governing the photoexcited carrier relaxation phenomena in heavy electron systems, we have also performed excitation intensity dependence studies on the heavy electron metal $YbAgCu_4$ and the Kondo insulator SmB_6. In both cases the relaxation rate, as well as the amplitude of the transient, was found to depend on the excitation fluence. Again, a striking similarity between the two was observed.

Finally, while a similar temperature dependence of the relaxation rate was found in all compounds studied, a two-stage rise-time was observed in two of the heavy fermion metals studied, $YbAgCu_4$ and $CeCoIn_5$.

The data were analysed in terms of two competing theoretical models that have been developed to explain the anomalous temperature and excitation intensity dependence of the transient. The first [12] argues that the carrier relaxation dynamics are governed by a conventional electron–phonon thermalization, where electron–phonon scattering is strongly suppressed within the peak in the DOS at the Fermi level. The second assumes a clear gap in the density of states, where the carrier relaxation is governed by the presence of a phonon bottleneck [14]. While the former was able to account for the temperature dependence of the relaxation rate, the agreement of the model with the measured temperature and excitation intensity dependence of the amplitude was less satisfactory. Moreover, the model is unable to explain the peculiar two-stage rise-time dynamics observed at low temperatures and excitation intensities. On the other hand, the phonon bottleneck model is found to account for both

rise-time dynamics, as well as the temperature and excitation intensity dependence of both relaxation rate and the amplitude of the photoinduced absorption.

One of the remaining open questions that needs further elucidation is the nature of a broad distribution of relaxation rates obtained in some compounds. For example, the stretching parameter $p \approx 0.3$ in $YbCdCu_4$ suggests relaxation rates spanning over more than two orders of magnitude. While non-exponential time dependence is expected at high perturbation levels (in virtually any model), the fact that this behaviour persists at extremely low perturbation densities (the increase in electronic temperature after perturbation only by $\approx$1 K) is surprising. Unfortunately, it is hard to determine the possible microscopic mechanism responsible for this behaviour based on the systematics of the available data.

A detailed analysis of all the observables (amplitude, rise-time, decay time) as a function of temperature and excitation density suggests that the carrier relaxation dynamics in a wide class of heavy electron compounds (both metallic and insulating) are governed by the presence of a (pseudo)gap in the density of states near the Fermi level. It is natural to assume that hybridization of local moments and conduction electrons is the origin of this gap in the DOS, and a comparison of the gap values extracted from the fit to the model with published data seems to support this hypothesis. The data analysis implies that the gap is only weakly temperature dependent, which suggests that, in these materials, lattice effects are dominant.

Acknowledgments

We acknowledge useful discussions with Viktor V Kabanov and Stuart A Trugman, and thank Elbert Chia for critically reading the manuscript. We would also like to acknowledge Richard D Averitt, Keun H Ahn, Verner K Thorsmolle, Nelson O Moreno, Matthias J Graf, Kaden Hazzard, Eric D Bauer and Joe D Thompson for their contribution to the presented research. This work was supported by US–Slovenian collaboration grant BI-US/05-06/023, NATO grant EAP.RIG.98142 and US DOE LDRD program.

References

[1] Demsar J *et al* 1999 *Phys. Rev. Lett.* **82** 4918
[2] Kabanov V V *et al* 1999 *Phys. Rev.* B **59** 1497
[3] Demsar J *et al* 2003 *Phys. Rev. Lett.* **91** 267002
[4] Demsar J *et al* 1999 *Phys. Rev. Lett.* **83** 800
[5] Demsar J *et al* 2002 *Phys. Rev.* B **66** 041101
[6] Bobyrev Yu V *et al* 2005 *Quant. Electron.* **35** 720
[7] Dvorsek D *et al* 2002 *Phys. Rev.* B **66** 041101
[8] Averitt R D *et al* 2001 *Phys. Rev.* B **63** 140502
[9] Stevens C J *et al* 1997 *Phys. Rev. Lett.* **78** 2212
[10] Hewson A C 1993 *The Kondo Problem to Heavy Fermions* (Cambridge: Cambridge University Press)
Degiorgi L 1999 *Rev. Mod. Phys.* **71** 687
[11] Rajan V T 1983 *Phys. Rev. Lett.* **51** 308
[12] Demsar J *et al* 2003 *Phys. Rev. Lett.* **91** 027401
[13] Ahn K H *et al* 2004 *Phys. Rev.* B **69** 45114
[14] Demsar J, Thorsmolle V T, Sarrao J L and Taylor A J 2006 *Phys. Rev. Lett.* **96** 037401
[15] Rothwarf A and Taylor B N 1967 *Phys. Rev. Lett.* **19** 27
[16] Kabanov V V, Demsar J and Mihailovic D 2005 *Phys. Rev. Lett.* **95** 147002
[17] Mihailovic D and Demsar J 1999 *Spectroscopy of Superconducting Materials* (*ACS Symposium Series* vol 730) ed E Falques (Washington, DC: The American Chemical Society)
[18] Canfield P C and Fisk Z 1992 *Phil. Mag.* B **65** 1117
[19] Carlslaw H S and Jaeger J C 1985 *Conduction of Heat in Solids* 2nd edn (Oxford: Oxford University Press)
[20] Demsar J 2000 *DPhil Thesis* University of Ljubljana

[21] Hancock J N *et al* 2004 *Phys. Rev. Lett.* **92** 186405
[22] Golubkov A V *et al* 2001 *Phys. Solid State* **43** 218
[23] Burch K S *et al* 2006 unpublished
[24] Lindsey C P and Patterson G D 1980 *J. Chem. Phys.* **73** 3348
[25] Sarrao J L *et al* 1999 *Phys. Rev.* B **59** 6855
Graf T *et al* 1995 *Phys. Rev.* B **51** 15053
[26] Groeneveld R H M, Sprik R and Lagendijk A 1995 *Phys. Rev.* B **51** 11433 and the references therein
[27] Eesley G L *et al* 1983 *Phys. Rev. Lett.* **51** 2140
[28] Moreno N O *et al* 2005 *Phys. Rev.* B **71** 165107
[29] Christianson A D *et al* 2005 *Phys. Rev.* B **72** 081102
[30] Petrovic C *et al* 2001 *J. Phys.: Condens. Matter* **13** L337
Movshovich R *et al* 2001 *Phys. Rev. Lett.* **86** 5152
[31] Kim J S *et al* 2001 *Phys. Rev.* B **64** 134524
[32] Nakatsuji S *et al* 2002 *Phys. Rev. Lett.* **89** 106402
[33] Nakatsuji S, Pines D and Fisk Z 2004 *Phys. Rev. Lett.* **92** 016401
[34] Riseborough P S 2000 *Adv. Phys.* **49** 257
[35] Nyhus P *et al* 1997 *Phys. Rev.* B **55** 12488
[36] Sarrao J L *et al* 1996 *Phys. Rev.* B **54** 12207
[37] Demsar J *et al* unpublished
[38] Anderson P W 1961 *Phys. Rev.* B **54** 12207
[39] Anisimov S I, Kapeliovich B L and Perel'man T L 1974 *Sov. Phys.—JETP* **39** 375
[40] Kaganov M I, Lifshitz I M and Tanatarov L V 1957 *Sov. Phys.—JETP* **4** 173
[41] Allen P B 1987 *Phys. Rev. Lett.* **59** 1460
[42] Hase M *et al* 2005 *Phys. Rev.* B **71** 184301
[43] Elsayed-Ali H E *et al* 1987 *Phys. Rev. Lett.* **58** 1212
[44] Brorson S D *et al* 1990 *Phys. Rev. Lett.* **64** 2172
[45] Lawrence J M *et al* 2001 *Phys. Rev.* B **63** 054427
[46] Zherlitsyn S *et al* 1999 *Phys. Rev.* B **60** 3148
[47] Galli M, Marabelli F and Bauer E 1995 *Physica* B **206/207** 355
[48] Burch K S *et al* 2005 *Phys. Rev. Lett.* **95** 046401
[49] Schoenlein R W, Lin W Z, Fujimoto J G and Eesley G L 1987 *Phys. Rev. Lett.* **58** 1680
[50] Schneider M L *et al* 2002 *Europhys. Lett.* **60** 460
[51] Demsar J *et al* 2001 *Phys. Rev.* B **63** 054519
[52] Langenberg D N and Larkin A I (ed) 1986 *Nonequilibrium Superconductivity* (Amsterdam: North-Holland Physics Publishing)
[53] Kaplan S B *et al* 1976 *Phys. Rev.* B **14** 4854
[54] Joyce J J *et al* 1999 *Phil. Mag.* B **79** 1
[55] Nyhus P *et al* 1997 *Phys. Rev.* B **55** 12488 and the references therein